Canadian Science Publishing
NRC Research Press journals | Publishing Services

Canadian Geotechnical Journal
Revue canadienne de géotechnique

Peak Punch-Through Capacity of Spudcan in Sand with Interbedded Clay: Numerical and Analytical Modelling

Journal:	*Canadian Geotechnical Journal*
Manuscript ID	cgj-2016-0597.R1
Manuscript Type:	Article
Date Submitted by the Author:	19-Jan-2017
Complete List of Authors:	Ullah, Shah Neyamat; National University of Singapore, Civil and Environmental Engineering Hu, Yuxia; University of Western Australia,
Keyword:	Finite element modelling, Centrifuge testing, peak bearing capacity, punch-through failure, sand with interbedded clay

Title: Peak Punch-Through Capacity of Spudcan in Sand with Interbedded Clay: Numerical and Analytical Modelling

Authors

i) Shah Neyamat Ullah (author of correspondence)
PhD
Research Fellow, Department of Civil and Environmental Engineering
National University of Singapore, 1 Engineering Drive 2, 117576.
Former PhD student, COFS, University of Western Australia
Email: shahneyamat.ullah@nus.edu.sg

ii) Yuxia Hu
PhD
Professor, School of Civil, Environmental and Mining Engineering
University of Western Australia
Crawley, Perth 6009.
Email: yuxia.hu@uwa.edu.au

Words (Intro-conclusion): 7000
Abstract: 170
Figures: 16
Table: 5

Peak Punch-Through Capacity of Spudcan in Sand with Interbedded Clay: Numerical and Analytical Modelling

Shah Neyamat Ullah and Yuxia Hu

ABSTRACT:

The presence of a thin soft clay layer inside a bed of sand may significantly reduce the bearing capacity of the sand layer imposing a risk of punch-through failure. In this paper, finite element (FE) simulations are reported using a hardening soil (HS) model for sand. The FE model has been verified against centrifuge tests involving loose and dense sand layers overlying clay soil. The effects of sand stiffness, foundation roughness, sand friction angle, undrained clay strength, clay strength non-homogeneity, and sand and clay layer geometries on the foundation peak capacities have been studied. Punch-through failure is initiated with an inclined sand plug being sheared and pushed into the underlying soft clay. During punch-through, the clay layer fails due to significant radial squeezing. Existing analytical models do not capture the combined failure mechanism of sand shearing and clay radial squeezing. A new analytical model is developed to estimate the peak punch-through capacity of a spudcan in sand with an interbedded clay layer showing improved performance over the current industry guidelines.

Keywords: Finite element modelling, centrifuge testing, peak bearing capacity, punch-through failure, sand with interbedded clay, spudcan

INTRODUCTION

Hydrocarbon extraction from shallow to medium water depth (up to ~150 m) is carried out using jack-up rigs commonly supported by three independent retractable truss legs. The quasi-circular conical foundations positioned at the end of each truss leg are normally referred to as spudcan. Punch-through of the foundation may take place when a strong layer (sand or stiff clay) overlies a relatively weaker layer when the preload exceeds the available soil bearing capacity, potentially destabilising the jack-up structure (Baglioni et al. 1982). To prevent the punch-through failure of the spudcan or to assess its potential, it is important to predict the ultimate or peak bearing capacity (q_{peak}) accurately (Figure 1c).

Contemporary works on foundation punch-through failure were mainly concerned with two-layer sand-clay or clay-clay stratigraphies (Teh et al. 2009; Hossain and Randolph 2010; Lee et al. 2013b; Hu et al. 2014). One major limitation of these studies is that their application is limited to cases where the underlying clay layer is of significant thickness.

Multi-layered soils (with three layers or more) place greater difficulties in bearing capacity assessment for offshore jack-up foundations. An improved understanding is required on how the different layers interact with each other hence contribute to the foundation capacity. Recently, some studies were reported in this area through physical modelling in a centrifuge (Hossain 2014; Ullah et al. 2016a). A comprehensive analytical model was presented in Ullah et al. (2016b) for spudcan installation in a clay bed with interbedded sand (i.e. clay-sand-clay) where a method of predicting the complete load-penetration profile was proposed.

The spudcan bearing capacity can be significantly reduced when a clay layer is interbedded in a sand layer (see Figure 1, where d_{peak} and d_{punch} represent the penetration depth at q_{peak} and the punch-through depth respectively). The punch-through severity, hence the d_{punch}, is a function of the location (i.e. depth from the seabed) and thickness of the soft clay layer. Accurate prediction of q_{peak} can increase the certainty in assessing (i) the potential of punch-through failure (i.e. if

q_{peak} > preloading pressure, the punch-through failure will not occur and vice versa), and (ii) the punch-through depth (i.e. if q_{peak} < preloading pressure).

There is a lack of understanding of the governing mechanisms controlling q_{peak} during punch-through in sand-clay-sand soil profiles. As a result, as far as the authors' knowledge, there is no analytical model that reliably and accurately predicts the spudcan peak bearing capacity (q_{peak}). Moreover, when the interbedded clay layer is located at a sufficient depth from the surface of the top sand layer (i.e. seabed), the clay layer may have little or no influence to the surface foundation bearing capacity. Hence, a potential design benefit may be gained by assessing the initial foundation capacity based on the sand characteristics alone, where calculations are greatly simplified. Thus, the critical depth and thickness of the interbedded clay layer, that influence the spudcan peak capacity, need to be investigated. Very limited guidance is presented in the current industry guidelines as documented in ISO (2012) on the aforementioned issues concerning sand with interbedded clay.

This paper studies the ultimate capacity of surface spudcan foundation in sand-clay-sand soils. The following sections report the numerical analysis results and the development of an analytical model based on the soil failure mechanisms observed in the numerical analysis.

FINITE ELEMENT MODEL AND MESH

For simplicity, the spudcan is modelled as a conical foundation with an included angle β of 154^o and diameter D of 12 m (Figure 2). Such included angle and size are typical of the Marathon LeTourneau design class spudcans as illustrated in Menzies and Roper (2008) and widely used in centrifuge experiments at UWA (Lee et al. 2013a; Ullah et al. 2016a).

The soil domain was discretised using 15-noded two-dimensional axisymmetric triangular elements. To minimise the soil-boundary interaction the lateral boundary was placed at 5D from the centre of the foundation following recommendations of Ullah et al. (2016c). Details of the FE model are given in Figure 2. Displacement-controlled analysis was conducted to obtain the ultimate spudcan capacity (q_{peak}), where the load-displacement curves in terms of q_{nom}-d/D reached a plateau, where q_{nom} (= F/A) is the nominal bearing pressure defined as the vertical reaction load (F) divided by the foundation base area ($A = \pi D^2/4$) and d is the penetration depth.

To find an optimum mesh, mesh sensitivity analyses were conducted for a spudcan (idealised as a conical foundation) and flat footing in loose and dense sand overlying clay soil profiles. For the former, the geometry and material properties were set up corresponding to the test L1SP4 reported by Hu et al. (2014) (Figure 3a) where q_{peak} in the centrifuge test was measured as 294 kPa (D = 12 m, $H_s/D = 0.5$, $H_c/D = \infty$, sand-clay intercept strength $s_{uo} = 12.96$ kPa, clay strength gradient $\rho = 1.54$ kPa/m and relative density $I_D = 44\%$). The total number of elements within the domain varied from coarse (316 elements) to super fine (1145 elements). The load-penetration curves indicate that the difference in peak capacity between a coarse and super fine mesh is only ~10 kPa (i.e. 3.7%). Balancing computational accuracy and efficiency, the fine mesh (Figure 3b with 776 elements) is seen to be adequate in providing a reasonable estimate of q_{peak}, which for this particular case is only 9% below the centrifuge test result. Further mesh sensitivity analyses in dense sand over clay (for test D1F30a reported in Lee et al., 2013a) and in sand-clay-sand provided greater accuracy (q_{peak} predicted within 4%). Therefore, the fine mesh was selected as the optimum for all the following analyses.

Constitutive model

To model the stress dependent response of sand, the hardening soil (HS) model is utilised in the current study. A full detailed description of the model including verification analysis is given in Schanz et al. (1999). Compared to the simple MC (Mohr-Coulomb) model the HS model allows the use of a stress dependent Young's modulus (E). Under a drained triaxial condition the following hyperbolic relationship is used (Kondner 1963)

$$E = 2E_{50}\left(1\text{-}R_f\frac{q}{q_f}\right) \text{ where, } E_{50} = E_{50}^{ref}\left(\frac{\sigma'_3}{p_{ref}}\right)^m \qquad 1$$

where, q is the deviatoric stress and q_f is the deviatoric stress at failure. R_f is the failure ratio usually taken as less than unity (set as 0.9 in all the analyses here). E_{50}^{ref} is the modulus of elasticity value at a reference confining pressure $p_{ref,}$ usually determined when q reaches 50% of q_f. σ'_3 is the minor effective principal stress and m is an exponent controlling the amount of stress dependency. For sand, m = 0.5 may be used (Suryasentana and Lehane 2014). A detailed parametric study on the effects of E_{50}^{ref} and m on q_{peak} is discussed shortly. Plastic strains due to

primary compression are controlled by the odometer stiffness E_{oed}^{ref}, which is similar in magnitude to E_{50}^{ref} (Plaxis 2014). Additional details of the model including formulation, verification and model data calibration can be found in Surarak et al. (2012).

The unloading and reloading within the current yield surface are assumed to be elastic and controlled by the stiffness E_{ur}^{ref}, which is typically taken as three times of E_{50}^{ref}(www.plaxis.nl). Failure occurs according to the MC failure criterion where the peak operative friction angle (φ'), dilitancy angle (ψ) and constant volume friction angle (φ_{cv}) are related by the following equation,

$$\sin\varphi_{cv} = \frac{\sin\varphi' - \sin\psi}{1 - \sin\varphi'\sin\psi} \qquad 2$$

A dilitancy cut-off is activated once the maximum porosity is reached requiring the input of the initial void ratio e_o, maximum (e_{max}) and minimum (e_{min}) void ratios. In the current study, e_0 = 0.5, e_{max} = 0.74 and e_{min} = 0.45 are selected since they are typical of UWA silica sand and other sands of sub-angular and sub-rounded uniform graded particles (Lee 2009; Suryasentana and Lehane 2014). For normally consolidated clay, a linear-elastic perfectly-plastic (EP) model with Tresca failure criterion is used to simulate its undrained behaviour. Table 1 lists all the soil parameters and their selected values.

Verification of numerical model against centrifuge test results in sand over clay soils

q_{peak} from the FE analysis have been verified against six centrifuge test results reported in Lee et al. (2013a) and Hu et al. (2014) for sand over clay stratigraphy. Table 2 shows the test case setups of these experiments, which include both dense and loose sand conditions. The operative friction (φ') and dilation angles (ψ) for input into the HS model were calculated according to the modified Bolton's (1986) equations as suggested in Lee et al. (2013b). In all cases the spudcan foundations (typically with a protruding spigot) were idealised as a conical foundation with diameter equal to the spudcan but with an equivalent included angle β (calculated according to

the approach suggested by Martin 1994), which for spudcan and flat circular foundation was 154^o and 180^o respectively.

Figure 4 depicts the comparison between the q_{peak} predicted by the FE analysis and that measured in the centrifuge experiments. Very good agreement is obtained with most of the data points fall closely to the line of equity (i.e. within 10% difference) with a maximum variation of ~ 20 %.

PARAMETRIC STUDY

Table 3 lists all the cases in the parametric study. The numerical simulations are grouped by their study focus for ease of reference in the discussion below.

Preliminary study on sand reference stiffness and foundation interface strength

Effect of sand stiffness parameters

The sand stiffness is dependent on two parameters: E_{50}^{ref} - the modulus of elasticity at p_{ref} (reference mean stress), and m – the exponent in Equation 1. The results revealed that (tests G1 in Table 3**)** progressively stiffer responses are measured for increasing E_{50}^{ref} (consistent with increasing sand density) with minimal impact on q_{peak}. These findings are in agreement with that reported in Yu et al. (2012) for small strain analysis. Similarly for the m parameter, q_{peak} was found to be only slightly affected by varying m from 0-1 (tests G2 in Table 3). m = 0.5 has been suggested by Yu et al. (2012) and Suryasentana and Lehane (2014) for use in FE modelling. Thus the medium values of E_{50}^{ref} = 24 kPa and m = 0.5 are adopted for sands in all the following analyses.

Effect of foundation-soil interface strength (R_{inter})

The foundation roughness has a significant effect on the penetration resistance in sand where the value of $N\gamma$ for a fully rough foundation (R_{inter} = 1) is approximately twice of that for a fully smooth (R_{inter} = 0) foundation (Chen 1975; Cassidy and Houlsby 2002). R_{inter} is the ratio of the shear strength of the interface to that of the surrounding soil. Figure 5 displays the effect of the foundation-soil interface roughness on the foundation peak capacity (q_{peak}) in sand-clay-sand soils with the top sand layer thickness varying as H_s/D = 0.25-∞, while H_c/D = 0.5, $\varphi' = \varphi_b' =$

30^o, $\psi = \psi_b = 2^o$ and $s_u = 10$ kPa (tests G3 Table 3). Adopting $R_{inter} = 0$ causes numerical instabilities due to the possibility of generating gaps along the interface (see www.plaxis.nl). Hence a small value of $R_{inter} = 0.2$ is chosen to model the smooth foundation. From Figure 5a, it can be seen that all the bearing capacity curves reach their ultimate values prior to 0.2D penetration (marked by a flat plateau), except for the rough foundation cases with a thicker top sand layer ($H_s/D \geq 1.5$). For cases with no clear indication of the ultimate capacity, the foundation capacity at $d/D = 0.2$ is used as q_{peak}. It is apparent that the interface roughness has no significant effect on q_{peak} when the top sand layer is relatively thin ($H_s/D < 1$). For $H_s/D = 1.5$, q_{peak} for a rough foundation is ~ 46% higher than that of a smooth foundation. From Figure 5b it is seen that for a smooth foundation once $H_s/D = 1.5$, q_{peak} equates the single layer sand capacity q_{sand} (i.e. $H_s/D = \infty$). This suggests that the underlying clay layer will have no effect for a smooth foundation once H_s/D reaches an upper bound of 1.5, as the failure mechanism is fully contained within the top layer. For a rough foundation this upper bound of H_s/D is equal to 2 as seen in Figure 5b.

Soil displacement vectors for surface spudcan with a relatively thin top sand layer of $H_s/D = 0.65 < 1$ are shown in Figure 6a. The soil flow mechanisms are nearly identical for both smooth and rough foundations, where punching shear failure in the top sand layer is apparent with a moderate amount of load spread. The shearing sand block, moving with the foundation, is pushed into the underlying clay (Vesic 1975). Thus the bearing capacities of both smooth and rough foundations are the same (see Figure 5).

Once the top sand layer becomes thicker i.e. $H_s/D > 1$, Figure 6b shows the soil failure mechanisms with the top sand layer of $H_s/D = 1.5$. The failure mechanisms for smooth and rough foundations are clearly different. The rough foundation directs soil to a much greater depth than the smooth foundation, effectively enlarging the failure mechanism generating a greater penetration resistance (see Figure 5). From these analyses, it is apparent that when the top sand layer is thin ($H_s/D < 1$), the punching shear failure mechanism in the top sand layer is dominant. Therefore, the foundation roughness plays an insignificant role on the peak capacity. This finding is also supported by finite element limit analyses by Shiau et al. (2003). At the same time, when the top sand layer becomes thicker ($H_s/D > 1$), the choice of an appropriate roughness coefficient becomes important in evaluating the foundation peak capacity.

Layer thickness effects: H_s and H_c

Effect of H_s/D *and* H_c/D *on* q_{peak}

The effects of the top sand and the middle clay layer thicknesses on the peak bearing capacity q_{peak} for a rough foundation are plotted in Figure 7 (G4 and G5 in Table 3). With increasing H_s/D, q_{peak} increases exponentially first and then progressively approaches the single sand layer capacity (Figure 7a). When the top sand layer thickness reaches $H_s/D = 2.0$, $q_{peak} = q_{sand}$ and the underlying clay layer is sufficiently distanced from the foundation base and therefore has no effect on q_{peak}. An opposite trend exists when q_{peak} is plotted against H_c/D (see Figure 7b). With increasing H_c/D, q_{peak} is found to reduce and progressively approaches the spudcan capacity of a sand overlying clay stratigraphy (i.e. $H_c/D \sim \infty$). When the middle clay layer becomes thinner ($H_c/D < 0.5$), its influence diminishes with q_{peak} increasing with decreasing H_c/D. With the disappearing middle clay layer (i.e. $H_c/D \rightarrow 0$), the foundation peak capacity approaches that of a single sand layer (q_{sand} in Figure 7a) and the top and bottom sand layers merge. However, the large difference between the q_{sand} and q_{peak} at $H_c/D = 0.15$ indicates that even a thin clay layer ($H_c/D < 0.5$) can provide a great reduction in foundation capacity relative to q_{sand}. Thus it is vitally important to detect the interbedded clay layer when it is close to the surface foundation (i.e. $H_s/D < 2$), even if it is thin ($0 < H_c/D < 0.5$). More discussion on this is detailed in the following session on the effect of H_c/D on the soil failure mechanism.

The foundation capacities (q_{sand}) on a single sand layer from the current study (i.e. $H_s/D = \infty$, test G4-T9 of Table 3) are compared with existing solutions from the literature. The comparison results are listed in Table 4 for the sand operative friction angle (φ') of 30^o. Both smooth and rough interfaces are simulated in the current FE analysis for spudcan with a conical base.

The existing methods overpredict q_{sand} over a range of 20-154% for a rough spudcan and 66-120% for a smooth spudcan. The differences among the solutions are attributed to the different failure mechanisms considered (Prandtl or Hill mechanism and different shapes of the trapped wedge) and due to different numerical schemes applied to solve the equations involved in lower and upper bound formulations (see Hjiaj et al. 2005 for a more comprehensive discussion). Lee et al. (2013b) showed that the Hansen's (1970) solution (which is also adopted in ISO, 2012)

gives a reasonable upper bound (q_{sand}) on the bearing capacity for sand over clay soils over the practical range of punch-through scenarios (i.e. $H_s/D < 1$). The same is also assumed herein for the analytical derivation presented later for sand with an interbedded clay layer.

Effect of* H_s/D *on soil failure mechanism

By varying the normalised top sand layer thickness H_s/D, three types of failure mechanisms are observed in Figure 8 (tests G4 in Table 3). Type I (Figure 8a) – general clay failure mechanism: with a very thin layer of top sand ($H_s/D \leq 0.15$), the thin top sand layer, together with the foundation, acts as part of the surface foundation, punching into the underlying clay layer. A general failure mechanism for a surface footing appears in the clay layer as the clay layer ($H_c/D \geq 0.5$) is thick enough for it to occur and the surcharge loading from the top sand layer is not very high. Type II (Figure 8b) – squeezing clay failure mechanism: with top sand layer thickness in the range of $0.15 < H_s/D < 1.5$, the punching shear failure mechanism in the top sand layer is apparent, which is also observed by others for foundation on sand over clay soils (Craig and Chua 1990; Teh et al. 2008; Hu et al. 2014). However, due to the higher surcharge above the clay layer and smaller layer thickness, the clay layer displays a radial squeezing mechanism (Figure 8b). Type III (Figure 8c) – general sand failure mechanism: when the top sand layer becomes thicker as $H_s/D \geq 2$, the soil failure mechanism is confined within the top sand layer and is independent of the underlying clay and sand layers, such confinement of soil failure mechanism in a thick sand layer is also observed in the PIV (particle image velocimetry) centrifuge tests reported by Teh (2007).

***Effects of friction and dilation angles of sand on* q_{peak}**

To investigate the effect of sand density on the foundation peak capacity, the top and bottom sand layer operative friction angle (φ') was varied over the range of 30^o-40^o with dilation angle (ψ) being calculated using Equation 2 inducing a range of 0^o-12.1^o and constant volume friction angle (φ_{cv}) being a constant of 30^o (tests G6 and G9 in Table 3). The top sand layer and middle clay layer thicknesses were fixed at $H_s/D = 0.5$ and $H_c/D = 0.25$ and the clay strength $s_u = 10$ kPa. As shown in Figure 9, q_{peak} increases with increasing φ' in the top sand layer. The soil failure mechanisms at q_{peak} in all four cases (loose to dense sand) display Type II failure mechanism as observed in Figure 8b. This is also in agreement with failure mechanisms

reported for sand over clay soils with dense sand (I_D = 85%) and medium dense sand (I_D = 44%) in the centrifuge tests by Teh et al. (2008) and Hu et al. (2014).

However, the sand operative friction angle (φ'_b) in the bottom sand layer shows no obvious effect on q_{peak} as seen in Figure 9. In other words, the surface foundation peak bearing capacity in sand-clay-sand stratigraphy is independent of the frictional strength properties of the bottom sand layer. This finding provides the basis for developing the analytical model below since the model only needs to involve the top sand and the interbedded clay layer.

Effect of clay thickness **H_c/D** ***on soil failure mechanism***

With a constant top sand layer thickness of H_s/D = 0.5, there are two failure mechanisms observed by varying the middle clay layer thickness (tests G5 in Table 3). The soil flow mechanisms are displayed in Figures 10a and 10b (where $\dot{\gamma}$ is the incremental shear strain). Figure 10a shows that when the clay layer is relatively thick as $H_c/D > 0.5$, Type I failure mechanism is apparent, i.e. general clay failure mechanism with surcharge from the top sand layer (see Figure 8). A triangular wedge is clearly visible in the clay layer directly under the loading area with emanating radial shear zones. The mechanism is in a good agreement with that observed in visual image PIV analysis from the centrifuge tests reported by Teh et al. (2008) for sand overlying clay. For thick clay layer of $H_c/D > 0.5$, the Type I failure mechanism can be maintained. The foundation peak capacity (q_{peak}) becomes constant with further increasing H_c/D and attains the peak capacity of foundation on two-layer sand over clay soils (see Figure 7b).

However, when the clay layer becomes thin as $H_c/D \leq 0.5$, the formation of the general clay failure mechanism is precluded. Thus, Type II failure mechanism is obtained, i.e. the squeezing clay failure mechanism (Figure 10b). According to the squeezing model presented by Meyerhof and Chaplin (1953), the bearing pressure due to squeezing is inversely proportional to H_c/D. This means that progressively smaller H_c/D will yield greater bearing pressure and vice versa, which is shown in Figure 7b. However, the existence of the thin clay layer constrains the soil failure mechanism to the clay layer with minimal deformation observed in the bottom sand layer. This constraint will remain regardless of how thin the clay layer is as long as $H_c/D > 0$. This means as long as a thin clay layer is present; the soil failure mechanism will not extend to the bottom sand

layer. This explains the reason of the large difference between the q_{peak} at $H_c/D \rightarrow 0$ and q_{sand} observed in Figure 7b. Although the q_{peak} increases with decreasing H_c/D due to the squeezing mechanism in the clay layer, the reduction in q_{peak} is expected to be larger when the clay layer is closer to the foundation (i.e. decreasing H_s/D in Figure 7a). Once the thin clay layer is far away from the surface foundation (i.e. $H_s/D > 2$), the thin clay effect on q_{peak} would disappear.

In view of the soil flow mechanisms, the bearing capacity q_{peak} is derived both from the top sand shear resistance and the underlying clay bearing capacity. It is important that any analytical model on q_{peak} can correctly model both the sand shear resistance as well as the clay bearing capacity.

Effect of undrained clay strength **(s_u)** ***and strength non-homogeneity*** **($\kappa = \rho D/s_u$) on q_{peak}**

The effect of s_u has been studied for two different normalised sand thicknesses (H_s/D) of 0.5 and 0.8 (Figure 11) with γ'_c being 7 kN/m^3, D = 12 m and s_u of 10, 20, 50 and 100 kPa (tests G7 of Table 3). It is seen that for any combination of H_s/D and H_c/D, the q_{peak} increases with increasing normalised undrained clay strength s_u/γ'_cD for both sand layer thicknesses of $H_s/D = 0.5$ and 0.8. However, when the sand layer thickness is kept constant of $H_s/D = 0.5$, Figure 11 reveals that q_{peak} increases with decreasing clay layer thickness of H_c/D for soft clay of $s_u/\gamma'_cD < 0.6$ ($s_u < 50$ kPa). This is also shown in Figure 7b for the same trend. Figure 10b displays the squeezing mechanism in the thin clay layer.

When the clay layer becomes stiff as $s_u/\gamma'_cD > 0.6$ ($s_u \geq 50$ kPa), the clay layer thickness of H_c/D has minimal influence on q_{peak}. This is because that a stiff clay layer (e.g. $s_u/\gamma'_cD = 1.19$ for s_u = 100 kPa) has a strength closer to the sand layers above and beneath it to allow the soil failure mechanism to be extended to the bottom sand layer. Evidence to support this is shown in Figure 12 comparing the soil vectorial displacements with a soft clay layer (s_u = 10 kPa, $s_u/\gamma'_cD = 0.12$) on the left and with a stiff clay layer (s_u = 100 kPa, $s_u/\gamma'_cD = 1.19$) on the right. It can be seen that while the soft clay layer squeezes out radially, the stiff clay layer shows less radial movement and more vertical movement causing some small displacements in the bottom sand layer. Therefore, the changing H_c/D over the range of 0.15-0.5 for stiff clays ($s_u \geq 50$ kPa; $s_u/\gamma'_cD \geq 0.6$) shows no appreciable increase in q_{peak}.

The effect of top sand layer thickness on q_{peak} can also be observed in Figure 11. When H_s/D increases from 0.5 to 0.8 and H_c/D is kept constant at 0.15, for relatively soft clays of s_u = 10 and 20 kPa, q_{peak} increases on average by ~ 93% and 95% respectively. For stiff clays of s_u = 50 and 100 kPa, the increase in q_{peak} is lower and about 67% and 44% respectively. This is because, with a soft clay layer, the soil failure mechanism is constrained by the location of the clay layer, hence q_{peak} is dependent on the mobilisation of the top sand layer strength, thus greater influence from H_s/D. However, with a stiff clay layer, the soil failure mechanism can be extended to the bottom sand layer, hence the influence from the top sand layer is reduced, but still significant.

As expected, for clay with strength increasing with depth q_{peak} progressively increases. For the two cases studied (tests G8 Table 1) q_{peak} is increased by ~20% when ρ is increased from 1 to 3 kPa/m (κ = 1.2-3.6).

It should be noted that, although very stiff clays are included in the numerical analysis for the completeness of this study, for offshore foundation punch-through failures, the clay layer is expected to be relatively soft.

ANALYTICAL MODELLING

Based on the parametric study above, three relevant zones for peak punch-through assessment is plotted in Figure 13. These zones are: Zone 1: when the sand layer is sufficiently thick (i.e. $H_s/D \geq 2$), q_{peak} is only dependent on the top sand layer; Zone 2: when the interbedded clay layer is thin (i.e. $H_c/D \leq 0.5$) the top sand is plugged into the underlying soft clay layer and the clay layer shows a radial squeezing mechanism; and Zone 3: when the middle clay layer is thick ($H_c/D > 0.5$) and the top sand layer is relatively thin ($H_s/D < 2$), a general bearing capacity failure in clay is expected. For this case, q_{peak} may be assessed by the mechanism proposed by Lee et al. (2013b) and Hu et al. (2014) for sand over clay soils. Notice that for Zone 1, the upper limit of H_s/D = 2 is derived from a rough foundation with relatively low sand friction and dilation angles as discussed before. For a smooth foundation this limit is lower (H_s/D =1.5). With relatively dense sands this limit might change and more investigation is required for a thorough assessment. When H_s/D >1, the peak bearing pressure is often high enough to support the operational loading of offshore jack-ups and punch-through are rarely reported for these cases

(Lee et al. 2013b). Hence for practical purpose, the cases with $H_s/D \leq 1.12$ and $H_c/D \leq 0.5$, which fall within Zone 2 are considered in the development of the analytical model below.

The analytical model is developed based on the previous UWA punch-through models of Lee et al. (2013b) and Hu et al. (2014) for spudcan on sand over clay soils. Following Lee et al. (2013b) at incipient failure, it is assumed that the sand frustum is pushed into the underlying clay layer at a load-spread angle being same as the sand dilitancy angle ψ. Where the clay layer fails due to radial squeezing when the normalised clay thickness is of $H_c/D \leq 0.5$ and the top sand layer thickness is of $H_s/D < 1.12$ (i.e. Zone 2 in Figure 13). It is assumed that the squeezing in clay occurs over a fictitious circular footing of diameter D', where D' is related to the sand thickness and sand dilitancy angle. The limit equilibrium of the conceptual model is illustrated in Figure 14.

According to Lee et al. (2013b), vertical force equilibrium of a thin horizontal disk element (shown as hatched in Figure 14) located at a depth z results in the following differential equation.

$$\frac{d\sigma_z^{'}}{dz}+\frac{E\tan\psi\sigma_z^{'}}{\frac{D}{2}+z\tan\psi}-\gamma_s^{'}=0 \qquad 3$$

where, σ'_z is the mean effective vertical stress acting on the thin disk element, ψ is the load-spread angle in sand (the same as the sand dilitancy angle), γ'_s is the sand effective unit weight and E is a simplification parameter given as,

$$E=2\left[1+D_F\left(\frac{\tan\varphi^*}{\tan\psi}-1\right)\right] \qquad 4$$

where, φ^* is a reduced operative friction angle accounting for the non-associated response of the sand obtained from the following expression provided in Drescher and Detournay (1993).

$$\tan\varphi^* = \frac{\sin\varphi'\cos\psi}{1-\sin\varphi'\sin\psi} \quad (5)$$

D_F is the distribution factor empirically related to H_s/D via two power relationships (Hu et al. 2015b) for spudcan and flat footing respectively as,

$$D_F(\text{spudcan}) = 0.642\left(\frac{H_s}{D}\right)^{-0.576}; 0.16 \le \frac{H_s}{D} \le 1.0 \quad (6)$$

$$D_F(\text{flat}) = 0.623\left(\frac{H_s}{D}\right)^{-0.174}; 0.21 < \frac{H_s}{D} < 1.12 \quad (7)$$

Hu et al. (2014) showed that the non-linear distribution factors adopted give an improved prediction of q_{peak} for both dense and medium dense sand overlying clay compared to the linear distribution factors recommended originally in Lee et al. (2013b).

Equation 3 can be integrated assuming D_F as constant with depth to give the following form of the solution.

$$\left(\frac{D}{2}+z\tan\psi\right)^{E}\sigma_z' = \frac{\gamma_s'\left(\frac{D}{2}+z\tan\psi\right)^{E+1}}{\tan\psi\left(E+1\right)}+C \quad (8)$$

where, C is an integration constant. In reality, the distribution factor D_F might vary with depth as a function of the accumulated radial and deviatoric shear strains at the foundation penetration level (Hu et al. 2016). However, for simplicity of the resulting q_{peak} equation, D_F is assumed constant herein. The integration constant C can be determined from the boundary condition that when z is equal to the effective sand thickness H_{eff} (refer to Figure 14), the mean vertical effective stress is equal to the limiting clay bearing pressure due to squeezing $q_{sq.}$

Following works of Meyerhof and Chaplin (1953) and Brown and Meyerhof (1969) q_{sq} can be expressed as,

$$q_{sq} = \left(5 + 0.33\frac{D'}{H_c}\right)s_u + q_o + \gamma'_s H_s \qquad 9$$

where, D' is the projected diameter on the sand-clay intercept and is given as,

$$D' = D + 1.76H_s \tan\psi \qquad 10$$

Equation 9 is also adopted in ISO (2012) to model squeezing in stiff over soft soil conditions. The last term in Equation 10 is the horizontal projection of the inclined shear surface where the factor 1.76 is resulted from the spudcan location at q_{peak}, which is taken as $0.12H_s$ as discussed below.

According to Teh et al. (2008), the mobilisation depth of the peak bearing capacity d_{peak} is related to the undisturbed sand thickness and can be taken as $0.12H_s$. This expression has been shown to work well for both dense and medium dense sand over clay conditions (Hu et al. 2014). Therefore, the effective sand thickness H_{eff} can be expressed as $0.88H_s$. At peak mobilisation, the penetration depth z is zero (Figure 14) and σ'_z equates q_{peak}. Substituting z = 0, $H_{eff} = 0.88H_s$ and putting the value of C in Equation 8 above, the equation for q_{peak} can be written as,

$$q_{peak} = \left[\left(5 + 0.33\frac{D'}{H_c}\right)s_u + q_o + 0.12H_s\gamma'_s\right]\left(1 + \frac{1.76H_s}{D}\tan\psi\right)^E + \frac{\gamma'_s D}{2\tan\psi(E+1)}\left[1 - \left(1 - \frac{1.76H_s}{D}E\tan\psi\right)\left(1 + \frac{1.76H_s}{D}\tan\psi\right)^E\right] \leq q_{sand} \qquad 11$$

for $\varphi' > \varphi_{cv}$. Where, q_o is the overburden pressure at the base of the foundation. Similarly for instances when $\varphi' = \varphi_{cv}$, q_{peak} is written as,

$$q_{peak} = \left[\left(5+0.33\frac{D'}{H_c}\right)s_u + q_o + 0.12H_s\gamma_s'\right]e^{E_o} + 0.88H_s\gamma_s'\left[e^{E_o}\left(1-\frac{1}{E_o}\right)+\frac{1}{E_o}\right] \le q_{sand} \quad (12)$$

where, E_o is given as,

$$E_o = 3.52D_F \sin\varphi_{cv}\frac{H_s}{D} \quad (13)$$

For clay with strength increasing with depth, s_u is taken at the mid-depth of the layer (i.e. $s_u = s_{uo} + \rho H_c/2$). The upper bound on Equation 13 and 14 is to ensure that q_{peak} does not exceed the ultimate bearing capacity of a single sand layer q_{sand} as given below,

$$q_{sand} = s_\gamma N_\gamma \frac{\gamma'_s D}{2} + s_q N_q q_o \quad (14)$$

where, the shape factors (s_γ, s_q) and bearing capacity factors (N_γ, N_q) are taken after Hansen (1970).

It can be readily seen from Equation 11 or 12 that for cases when H_c is zero (i.e. the soil profile becomes of single layer sand), $q_{peak} = q_{sand}$.

The operative friction (φ') and dilation angle (ψ) needed to calculate q_{peak} from Equation 11 or 12 are adopted from modified Bolton's (1986) strength-dilitancy relationships as given in Lee et al. (2013b) and reproduced below where the mean effective stress p_o' is replaced by q_{peak} and an iterative process is applied to arrive at the correct friction angle.

$$I_R = I_D(Q - \ln q_{peak}) - 1, \quad 0 \le I_R \le 4 \quad (15)$$

$$\varphi' = \varphi_{cv} + 2.65I_R \quad (16)$$

$$0.8\psi = \varphi' - \varphi_{cv}, \quad \psi \ge 0 \quad (17)$$

I_R is the strength dilitancy index, I_D is the sand relative density, Q is the natural logarithm of the grain crushing strength in kPa and φ_{cv} is the constant volume friction angle. In this way, the stress level dependency of the operative friction and dilation angles are captured simplistically. No design charts are required in calculating the peak capacity from Equation 11. Equation 11 or 12 and 15-17 can be conveniently coded into a spreadsheet program such as Microsoft Excel to perform the calculations.

Comparative performance of the ISO and developed model

The performance of the developed model is assessed in comparison to the load spread or projected area approach (PA) and the punching shear approach (PS) adopted in ISO (2012). Two different projected angles (α_p) have been considered for the load spread method corresponding to 1h:3v (18.43^o) and 1h:5v (11.31^o), where h means horizontal and v means vertical. The punching shear coefficient K_s is estimated from the chart provided in (ISO 2012) with the friction angle corresponding to that of the numerical tests (Table 3). As noted in Hu et al. (2015a) there might be some ambiguity in the ISO (2012) guidelines regarding calculation of the surcharge term for evaluating the bearing capacity of the larger fictitious footing in the projected area approach. Also here it is noted that for a very small undrained shear strength of the clay layer the sand frustum weight can be dominant over the clay bearing capacity given by the larger fictitious footing, resulting in a negative q_{peak} value (see Equation 20). For these reasons, to comprehensively assess the performance of the ISO models two variants of the projected area and punching shear equations were used.

For the projected area approach the following equation was used considering the weight of the sand frustum,

$$q_{peak} = \left[\left(1+2\frac{H_s}{D}\tan\alpha_p\right)^2\left(s_c N_c s_{uo} + q_o\right)\right] - \left[\left(1+2\frac{H_s}{D}\tan\alpha_p\right)^2 \gamma'_s H_s\right] \qquad 20$$

where, α_p is the projected angle, s_c is the shape factor and N_c is the shallow bearing capacity factor in clay and s_{uo} is the top sand-clay intercept strength ($s_{uo} = s_u$ when clay strength gradient $\rho = 0$). The last term vanishes without the sand frustum weight ($\gamma'_s = 0$).

For the punching shear approach, the following equation was used when considering the weight of the sand frustum,

$$q_{peak} = \left(s_c N_c s_{uo} + q_o\right) + \left[2\frac{H_s}{D}\left(\gamma'_s H_s + 2q_o\right)K_s \tan\varphi'\right] - \gamma'_s H_s \qquad 21$$

and when neglecting the sand frustum weight the last term vanishes.

A total of 29 numerical tests have been simulated assessing the performance of ISO and the proposed method. In this retrospective simulation, tests with $H_c/D \leq 0.5$ were mainly considered where a radial squeezing mechanism in the clay layer is expected to take place (detail test parameters were given in Table 3 and have been marked with an asterisk). Out of interest, three tests (G5 tests T5-T7 of Table 3) were included with H_c/D = 0.65-1 where a general bearing failure in clay is expected and the profile approach that of sand-clay (see Figure 7). In these tests, the top sand operative friction angle (φ') varied from 30^o-40^o i.e. both dense and loose sands have been considered. Undrained shear strength in clay (s_u or s_{uo}) varied over the range of 2-20 kPa with clay strength gradient (ρ) varying as 0 and 3 kPa/m. For clay with strength increasing with depth, s_u was taken as the average strength of the layer in the proposed method.

Figure 15 shows the performance of all the methods. It is evident that both the projected area approach and the punching shear approach are highly conservative in their estimation of the punch through capacity (q_{peak}). Such results were expected as neither the projected area approach nor the punching shear approach accurately models the stress level-dependent response in the sand layer as highlighted by a number of researchers (Teh 2007; Lee et al. 2013b; Hu et al. 2014; Hu et al. 2015a). When compared against a large number of centrifuge tests (71 in total) on sand over clay, Hu et al. (2015a) showed that the ISO methods of projected area and punching shear on average under predict the peak capacity by as high as 42% and 41% respectively. The level of conservatism is higher in this study involving sand-clay-sand with the average under prediction for the ISO methods of PA and PS being as high as 59% and 63% respectively for the 29 tests simulated.

The reason for this is, in addition to the conservative modelling of the sand shear resistance, a general bearing capacity failure (N_c = 6) is assumed in the clay layer by the ISO methods (i.e. the PA and PS methods). As the bearing capacity factor for squeezing (i.e. for thin layers) is significantly greater than N_c values obtained from conventional shallow bearing capacity analyses, this assumption in the ISO (both PA and PS) methods adds to the conservatism. The ISO (2012) code does not provide sufficient details regarding calculating peak punch-through capacity in three layer soils. To comprehensively assess the performance of the ISO approaches further calculation were performed by assuming squeezing in the clay layer (Figure 15a-c). Both the PA and PS methods give improved prediction (see Table 5) relative to the general bearing failure prediction, suggesting the importance of considering squeezing for thin clay layers. However, the predictions still fall outside the 20% bounds indicating conservative modelling of the sand shear resistance.

In the proposed model, by improving the sand shear resistance by correctly modelling the stress level dependency of the sand layer as well as accurate modelling of squeezing in the underlying clay layer significantly improves the prediction (Figure 15d). Interestingly, the three tests with $H_c/D > 0.5$ were predicted within 2.5% accuracy. This is because the resistance obtained from the squeezing model for thicker clay layers lies close to that obtained from general bearing capacity theory but differs significantly for thinner clay layers (ISO, 2012). Overall the average measured over predicted q_{peak} ratio is only 1.04 with a significantly lower standard deviation (SD) and coefficient of variation (COV) of 0.18 and 0.17 in comparison to the ISO approaches (see Table 5).

Parametric study on the new model

A parametric study is conducted as shown in Figure 16 using the developed q_{peak} Equations 13 and 14 and 17-19. Unless otherwise mentioned D is taken as 12 m, the sand relative density I_D is taken as 50% representing medium dense sand, $\varphi_{cv} = 30^o$, γ'_s = 10 kN/m^3, s_u = 10 kPa, ρ = 0 kPa/m and γ'_c = 7 kN/m^3. The thicknesses of the top sand and middle clay layers are set up as H_s/D = 0.17-1 and H_c/D = 0.08-0.5. Figure 16a and 16b shows that the model correctly captures the layer effects with q_{peak} increasing with H_s/D and decreasing with increasing H_c/D. For smaller H_c/D the model also correctly limits q_{peak} to its upper bound q_{sand}. For instance, when H_s/D =

0.17 (Figure 16b plus sign marker) and $H_c/D = 0.008$, q_{peak} was calculated as 790 kPa and q_{sand} was 720 kPa ($\varphi' = 31.8$, $\psi = 2.2$, $q_o = 0$) requiring limiting q_{peak} to 720 kPa. This limiting effect can also be seen for the case when $H_s/D = 1$ where a sudden drop in q_{peak} occur in regions where $H_c/D < \sim 0.05$. Any contemporary punch-through model including the ISO methods at best will only predict a straight line on the q_{peak}-H_c/D plane.

q_{peak} also increases with the top sand operative friction angle φ', dilation angle ψ and undrained clay strength s_u (Figure 16c -16e). q_{peak} obtained with φ' of 30^o-40^o and ψ of 0^o-12.1^o in the FE simulation (tests G6 of Table 3) agreeing exceptionally well with the model predictions (Figure 16c and 16d).

CONCLUSION

The peak capacity of a spudcan in sand with an interbedded soft clay layer (i.e. sand-clay-sand) has been studied utilising displacement finite element techniques with the hardening soil (HS) model for sand and a simple Tresca model for clay. The spudcan was idealised as a conical foundation with diameter D of 12 m and an included angle of 154^o. The effects of a series parameters of sand and clay on the foundation peak capacity has been studied extensively. The conclusions obtained are listed below.

- The soil stiffness parameters such as the reference modulus of elasticity (E_{50}^{ref}) and the stress dependency exponent parameter m only affect the load-penetration response at small strains and had no influence on the peak punch-through capacity (q_{peak}), which occur at relatively large strains.

- The foundation roughness only affects q_{peak} when the top sand layer is thick (i.e. $H_s/D > 1.0$) requiring an appropriate roughness factor. When the top sand layer is thin (i.e. $H_s/D \leq 1.0$), the foundation roughness shows no effect on q_{peak}.

- q_{peak} increase with increasing top sand layer thickness (H_s/D) and increasing top sand layer operative friction angle. q_{peak} reached the bearing capacity of a single layer of sand

(q_{sand}) once $H_s/D \geq 2$ for a rough foundation. For a smooth foundation this upper limit of H_s/D is reduced and can be taken as 1.5 over the range of material properties investigated.

- On the other hand, For sand-clay-sand, q_{peak} was found to increase with decreasing clay layer thickness (H_c/D) due to the radial squeezing mechanism in the soft clay layer under the conditions of $H_s/D < 1$ and $H_c/D < 0.5$. This trend has not been captured by any contemporary spudcan punch-through model. When the clay layer was thick (i.e. $H_c/D > 0.5$), a more general bearing capacity failure takes place in the underlying clay layer.

- For both thin and thick soft clay layers, q_{peak} was unaffected by the frictional properties of the bottom sand layer.

- The presence of a soft clay layer in a sand bed significantly reduces the peak bearing capacity compared to a single layer of sand without clay, when $H_s/D < 1$ and $H_c/D < 0.5$, due to the soil failure zone being limited to the depth of the soft clay layer. With the comparison to the foundation peak capacity in a single sand layer, the reduction on q_{peak} can be as high as 50% or higher, even if the soft clay layer was very thin (i.e. $H_c/D < 0.1$). Thus, it is vitally important to detect the soft clay layer in the field.
- An analytical prediction model was proposed based on the failure mechanisms observed in the numerical simulations and the limit equilibrium principle. The model was verified by 29 numerical tests covering a wide range of normalised geometries and material strength properties providing excellent performance with q_{peak} being predicted mostly within 20% bound. The model also showed much improved prediction on q_{peak} when compared with the ISO models.

ACKNOWLEDGEMENTS

The dedicated support from staff at Plaxis Netherland is gratefully acknowledged. The authors would also like to thank Dr Yusuke Suzuki from the Norwegian Geotechnical Institute (NGI) for the fruitful discussions over the course of this research.

REFERENCES

Baglioni, V.P., Chow, G.S., and Endley, S.N. 1982. Jack-Up Rig Foundation Stability in Stratified Soil Profiles. *In* Offshore Technology Conference, Houston, Texas, OTC 4409, pp. 363-384.

Bolton, M.D. 1986. The strength and dilitancy of sands. Géotechnique 36(1): 65-78.

Bolton, M.D., and Lau, C.K. 1993. Vertical bearing capacity factors for circular and strip footings on Mohr–Coulomb soil. Canadian Geotechnical Journal **30**(6): 1024-1033. DOI: 10.1139/t93-099.

Brown, J.D., and Meyerhof, G.G. 1969. Experimental study of bearing capacity in layered clays. *In* Proceedings of 7th international conference on soil mechanics and foundation engineering (ICSMFE), Mexico. pp. 45-51.

Cassidy, M.J., and Houlsby, H.T. 2002. Vertical bearing capacity factors for conical footings on sand. Géotechnique 52(9): 687-692.

Chen, W.F. 1975. Limit analysis and soil plasticity. Elsevier scentific publishing company, Newyork.

Craig, W.H., and Chua, K. 1990. Deep penetration of spudcan foundations on sand and clay. Géotechnique 40(4): 541-556.

Das, B. M. 2010. Geotechnical engineering handbook. J.Ross Publishing, pp. 1-800.

Drescher, A., and Detournay, E. 1993. Limit load in translational failure mechanisms for associative and non-associative materials. Géotechnique 43(3): 443-456.

Hansen, J.B. 1970. A revised and extended formula for bearing capacity. Bulleting of the Danish Geotechnical Institute, 28, 5-11.

Hjiaj, M., Lyamin, A.V., and Sloan, S.W. 2005. Numerical limit analysis solutions for the bearing capacity factor Nγ. International Journal of Solids and Structures **42**(5–6): 1681-1704. DOI: http://dx.doi.org/10.1016/j.ijsolstr.2004.08.002.

Hossain, M.S. 2014. Experimental investigation of spudcan penetration in multi-layer clays with interbedded sand layers. Géotechnique 64(4): 258-276.

Hossain, M.S., and Randolph, M.F. 2010. Deep-penetrating spudcan foundations on layered clays: centrifuge tests. Géotechnique 60(3): 157-170.

Hu, P., Stanier, S.A., Cassidy, M.J., and Wang, D. 2014. Predicting Peak Resistance of Spudcan Penetrating Sand Overlying Clay. Journal of Geotechnical and Geoenvironmental Engineering 140(2): 04013009. DOI:10.1061/(ASCE)GT.1943-5606.0001016.

Hu, P., Stanier, S.A., Wang, D., and Cassidy, M. 2015a. A comparison of full profile prediction methods for a spudcan penetrating sand overlying clay. Géotechnique Letters 5(3): 131-139. DOI:10.1680/jgele.15.00051.

Hu, P., Wang, D., Stanier, S. A. and Cassidy, M. J. 2015b. Assessing the punch-through hazard of a spudcan on sand overlying clay. Géotechnique 65(11): 883-896.

Hu, P., Stanier, S.A., Wang, D., and Cassidy, M. 2016. Effect of footing shape on penetration in sand overlying clay. International Journal of Physical Modelling in Geotechnics, 16(3), 119-133.

ISO. 2012. ISO 19905-1: Petroleum and natural gas industries- site specific assessment of mobile offshore units-Part 1 : Jack-ups. Geneva, Switzerland : International Organization for Standardization.

Kondner, R.L. 1963. Hyperbolic stress-strain response: cohesive soils. Journal of Soil Mechanics and Foundations Division, ASCE 89 (1963), 115-143.

Lee, K.K. 2009. Investigation of Potential Spudcan Punch Through Failure on Sand Overlying Clay Soils. PhD thesis, *In* School of Civil and Resource Engineering. University of Western Australia, Perth.

Lee, K.K., Cassidy, M.J., and Randolph, M.F. 2013a. Bearing capacity on sand overlying clay soils: experimental and finite-element investigation of potential punch-through failure. Géotechnique 63(15): 1271-1284.

Lee, K.K., Randolph, M.F., and Cassidy, M.J. 2013b. Bearing capacity on sand overlying clay soils: a simplified conceptual model. Géotechnique 63(15): 1285-1297.

Lyamin, A.V., Salgado, R., Sloan, S.W., and Prezzi, M. 2007. Two- and three-dimensional bearing capacity of footings in sand. Géotechnique **57**(8): 647-662.

Michalowski, R. 1997. An estimate of the influence of soil weight on bearing capacity using limit analysis. soils and foundations **37**(4): 57-64. DOI: 10.3208/sandf.37.4_57.

Martin, C.M. 1994. Physical and numerical modelling of offshore foundations under combined loads. PhD thesis, University of Oxford, UK.

Menzies, D., and Roper, R. 2008. Comparison of Jackup Rig Spudcan Penetration Methods in Clay. *In* Offshore Technology Conference, Houston, Texas. pp. 1-22.

Meyerhof, G.G., and Chaplin, T.K. 1953. The compression and bearing capacity of cohesive layers. British Journal of Applied Physics 4(1): 20-26.DOI:10.1088/0508-3443/4/1/305.

Meyerhof, G.G. 1963. Some Recent Research on the Bearing Capacity of Foundations. Canadian Geotechnical Journal **1**(1): 16-26. DOI: 10.1139/t63-003.

Plaxis (2014). Plaxis 2D AE version. web: www.plaxis.nl

Schanz, T., Vermeer, P.A., and Bonnier, P.G. 1999. The hardening soil model: formulation and verification. In Beyond 2000 in computational geotechnics: ten years of Plaxis International (ed.R. B. J. Brinkgreve), pp. 281–296. Rotterdam, the Netherlands:Balkema.

Shiau, J.S., Lyamin, A.V., and Sloan, S.W. 2003. Bearing capacity of a sand layer on clay by finite element limit analysis. Canadian Geotechnical Journal 40(5): 900-915.

Surarak, C., Likitlersuang, S., Wanatowski, D., Balasubramaniam, A., Oh, E., and Guan, H. 2012. Stiffness and strength parameters for hardening soil model of soft and stiff Bangkok clays. Soils and Foundations 52(4):682-697.

Suryasentana, S.K., and Lehane, B.M. 2014. Numerical derivation of CPT-based p–y curves for piles in sand. Géotechnique **64**(3): 186-194. DOI:10.1680/geot.13.P.026.

Teh, K.L., Leung, C.F., Chow, Y.K., and Handidjaja, P. 2009. Prediction of Punch-through for Spudcan Penetration in Sand Overlying Clay. *In* Offshore Technology Conference, Houston, Texas, OTC 20060, pp. 1-14.

Teh, K.L. 2007. Punch through of spudcan foundation on sand overlying clay. PhD thesis, National University of Singapore.

Teh, K.L., Cassidy, M.J., Leung, C.F., Chow, Y.K., Randolph, M.F., and Quah, C.K. 2008. Revealing the bearing capacity mechanisms of a penetrating spudcan through sand overlying clay. Géotechnique 58(10): 793-804. DOI: 10.1680/geot.2008.58.10.793.

Ullah, S.N., Stanier, S., Hu, Y., and White, D. 2016a. Foundation punch-through in clay with sand: centrifuge modelling. Géotechnique (in press).

Ullah, S.N., Stanier, S., Hu, Y., and White, D. 2016b. Foundation punch-through in clay with sand: analytical modelling. Géotechnique (in press).

Ullah, S.N., Hu, Y., White, D., and Stanier, S. 2016c. Lateral boundary effects in centrifuge spudcan foundation tests. International Journal of Physical Modelling in Geotechnics (available online ahead of print).

Vesic, A.S. 1975. Foundation engineering handbook, Van Nostrand Reinhold, New York, pp. 121-147.

Yu, L., Hu, Y., Liu, J., Randolph, M.F., and Kong, X. 2012. Numerical study of spudcan penetration in loose sand overlying clay. Computers and Geotechnics 46(2012):1-12.DOI:http://dx.doi.org/10.1016/j.compgeo.2012.05.01.

Figure Captions

Figure 1. In-situ offshore soil profiles with interbedded sand and clay layers: a) offshore southeast Asia, b) offshore South America (data from Teh et al. 2009 and Baglioni et al. 1982) and c) a typical load-penetration profile in sand-clay-sand soil.

Figure 2. Problem description and model setup.

Figure 3. a) Mesh sensitivity analyses on a loose sand overlying clay soil ($H_s/D = 0.5$, $H_c/D = \infty$, $\varphi' = 33.27^o$, $\psi = 2.84^o$) b) Optimum mesh with 776 elements.

Figure 4. Verification of the finite element model against model centrifuge experiments on sand overlying clay.

Figure 5. Effect of foundation roughness on the measured load-penetration response ($H_s/D = 0.25$-1.5, $H_c/D = 0.5$, $D = 12$ m, $\varphi' = \varphi'_b = 30^o$, $\psi = \psi_b = 2^o$, $s_u = 10$ kPa; tests G3 (T1-T4), G1 (T2, T6, T7), G4T2 of Table 3).

Figure 6. (a). Effect of foundation roughness on the failure mechanism for relatively thin top sand ($H_s/D = 0.65$, $H_c/D = 0.5$, $D = 12$ m, $\varphi' = \varphi'_b = 30^o$, $\psi = \psi_b = 2^o$, $s_u = 10$ kPa; tests G1T2 (rough) and G3T2 (smooth) of Table 3); (b). Effect of foundation roughness on the failure mechanism for relatively thicker top sand ($H_s/D = 1.5$, $H_c/D = 0.5$, $D = 12$ m, $\varphi' = \varphi'_b = 30^o$, $\psi = \psi_b = 2^o$, $s_u = 10$ kPa; tests G3T4 (smooth) and G4T7 (rough) of Table 3)..

Figure 7. Effect of normalised geometries on the peak punch-through capacity a) effect of H_s/D ($H_c/D = 0.5$, $D = 12$ m, $\varphi' = \varphi'_b = 30^o$, $\psi = \psi_b = 2^o$, $s_u = 10$ kPa; tests G4 of Table 3) and b) effect of H_c/D ($H_s/D = 0.5$, $\varphi' = \varphi'_b = 30^o$, $\psi = \psi_b = 2^o$, $s_u = 10$ kPa; tests G5 of Table 3).

Figure 8. Effect of normalised top sand thickness (H_s/D) on the observed failure mechanism: a) small H_s/D (= 0.15) b) intermediate H_s/D (= 0.65) and c) large H_s/D (= 2) (in all cases, $H_c/D = 0.5$, $D = 12$ m, $\varphi' = \varphi'_b = 30^o$, $\psi = \psi_b = 2^o$, $s_u = 10$ kPa; tests G4T1, G1T2, G4T8 of Table 3).

Figure 9. Effect of top and bottom sand operative friction and dilation angle on q_{peak} ($H_s/D = 0.5$, $H_c/D = 0.25$, $\varphi_{cv} = 30^o$, $s_u = 10$ kPa; tests G6 and G9 of Table 3)

Figure 10. (a). Effect of normalised clay thickness (H_c/D) on the failure mechanism: thick clay effect ($H_s/D = 0.5$, $H_c/D = 0.8$, $D = 12$ m, $\varphi' = \varphi'_b = 30^o$, $\psi = \psi_b = 2^o$, $s_u = 10$ kPa; test G5T6 of Table 3); (b) Effect of normalised clay thickness (H_c/D) on the failure mechanism: thin clay effect ($H_s/D = 0.5$, $H_c/D = 0.15$, $D = 12$ m, $\varphi' = \varphi'_b = 30^o$, $\psi = \psi_b = 2^o$, $s_u = 10$ kPa; test G5T1 of Table 3)

Figure 11. Effect of undrained clay strength s_u on q_{peak} ($H_s/D = 0.5$- 0.8, $H_c/D = 0.15$-0.25, $D = 12$ m, $\varphi' = \varphi'_b = 30^o$, $\psi = \psi_b = 2^o$, $s_u = 10$-100 kPa; tests G7 of Table 3).

Figure 12. Soil flow mechanisms: effect of s_u ($H_s/D = 0.5$, $H_c/D = 0.15$, $D = 12$ m, $\varphi' = \varphi'_b = 30^o$, $\psi = \psi_b = 2^o$, $s_u =$ 10kPa (left) and 100 kPa (right); tests G5T1 (left) and G7T9 (right) of Table 3).

Figure 13. Possible failure zones in sand with interbedded clay.

Figure 14 Analytical model of foundation bearing capacity in sand with a thin interbedded clay layer.

Figure 15. Performance of the developed model in comparison to ISO ($H_c/D \leq 0.5$): a) load spread approach (1h:3v), b) load spread approach (1h:5v), c) ISO punching shear approach, d) proposed method.

Figure 16. Effect of different parameters on q_{peak} in sand-clay-sand a) effect of H_s/D ($D = 12$ m, $I_D = 50\%$, $s_u = 10$ kPa, $\varphi_{cv} = 30^o$), b) effect from H_c/D ($D = 12$ m, $I_D = 50\%$, $s_u = 10$ kPa, $\varphi_{cv} = 30^o$), c) effect of top sand operative friction angle φ' ($H_c/D = 0.25$, $D = 12$ m, $I_D = 0.3$:0.05:0.99, $s_u = 10$ kPa, $\varphi_{cv} = 30^o$), d) effect of top sand dilation

angle ψ (H_c/D = 0.25, D = 12 m, I_D = 30% : 5% : 99%, s_u = 10 kPa, φ_{cv} = 30°) and e) effect of clay undrained shear strength s_u (H_c/D = 0.33, D = 12 m, I_D = 50%, φ_{cv} = 30°).

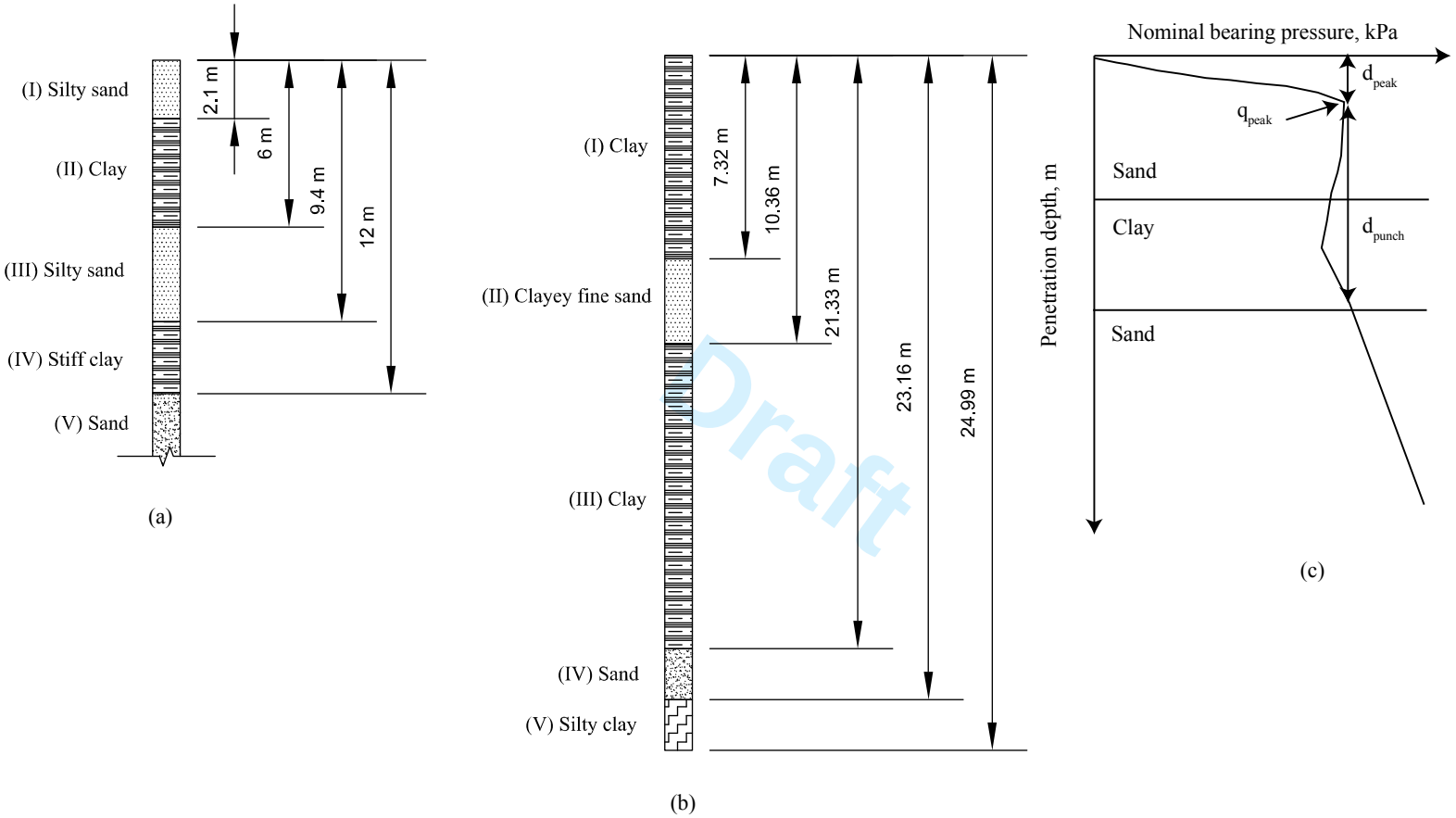

Figure 1 In-situ offshore soil profiles with interbedded sand and clay layers: a) offshore southeast Asia, b) offshore South America (data from Teh et al. 2009 and Baglioni et al. 1982) and c) a typical load-penetration profile in sand-clay-sand soil.

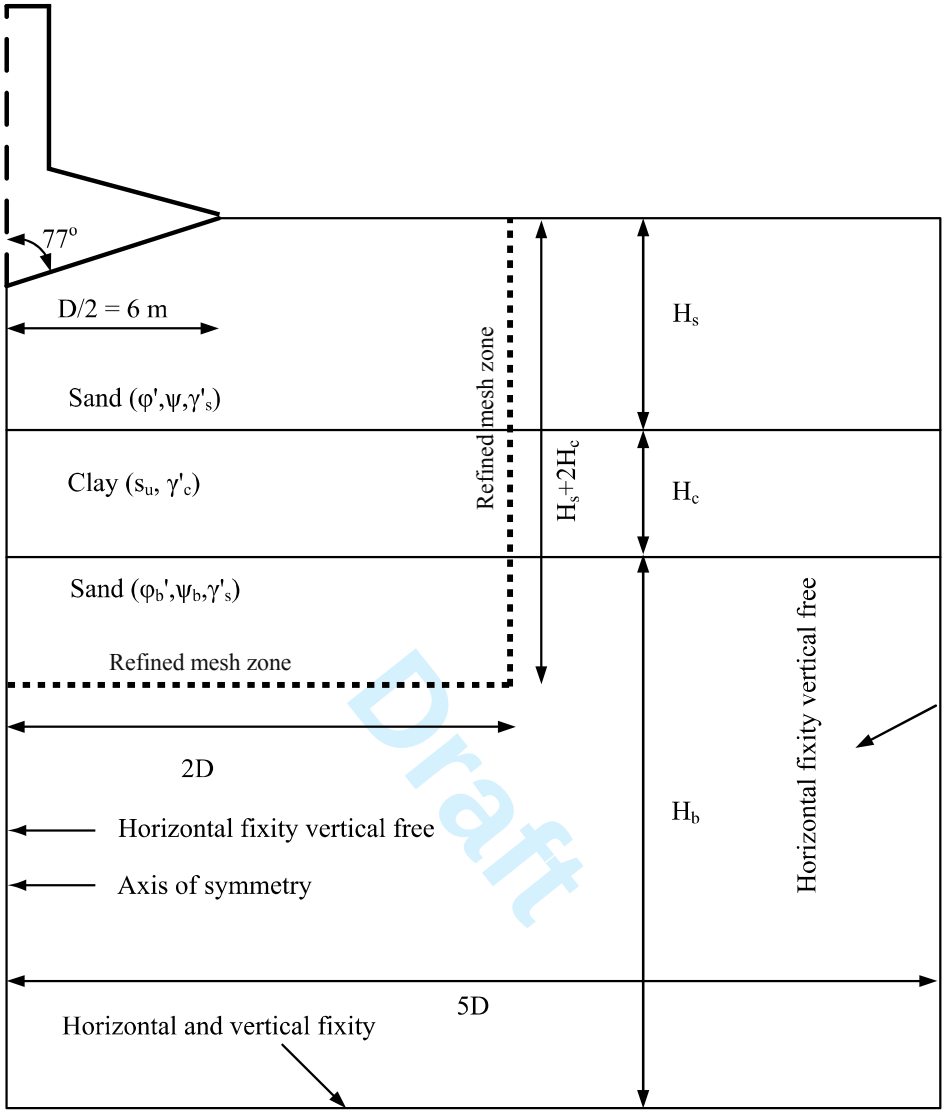

Figure 2 Problem description and model setup.

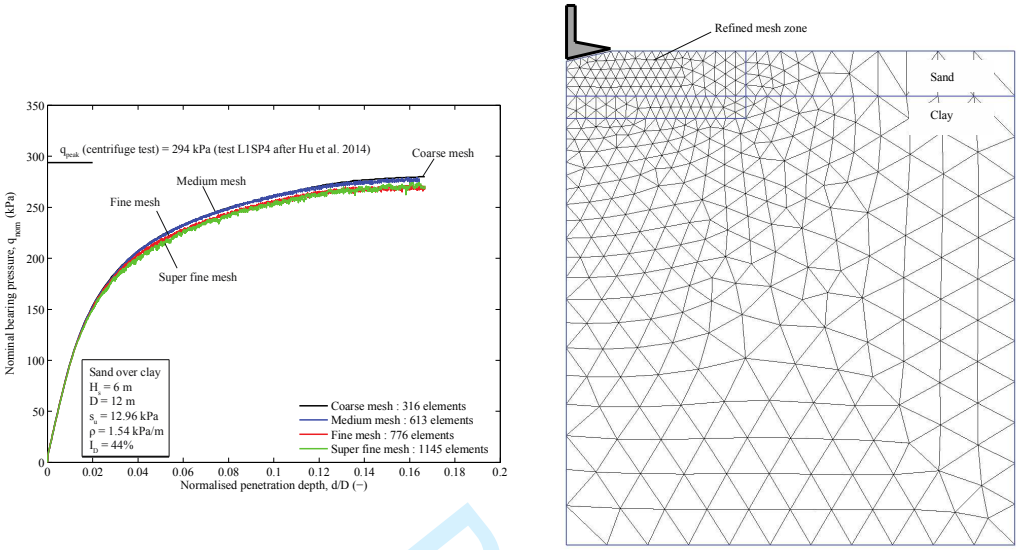

Figure 3 a) Mesh sensitivity analyses on a loose sand overlying clay soil ($H_s/D = 0.5$, $H_c/D = \infty$, $\varphi' = 33.27^o$, $\psi = 2.84^o$) b) Optimum mesh with 776 elements.

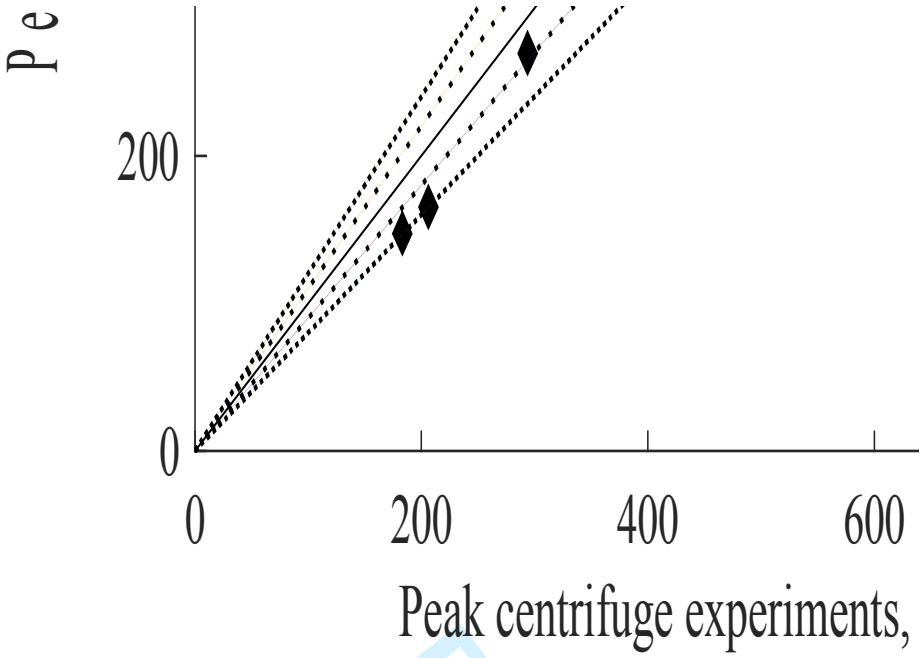

Figure 4 Verification of the finite element model against model centrifuge experiments on sand overlying clay.

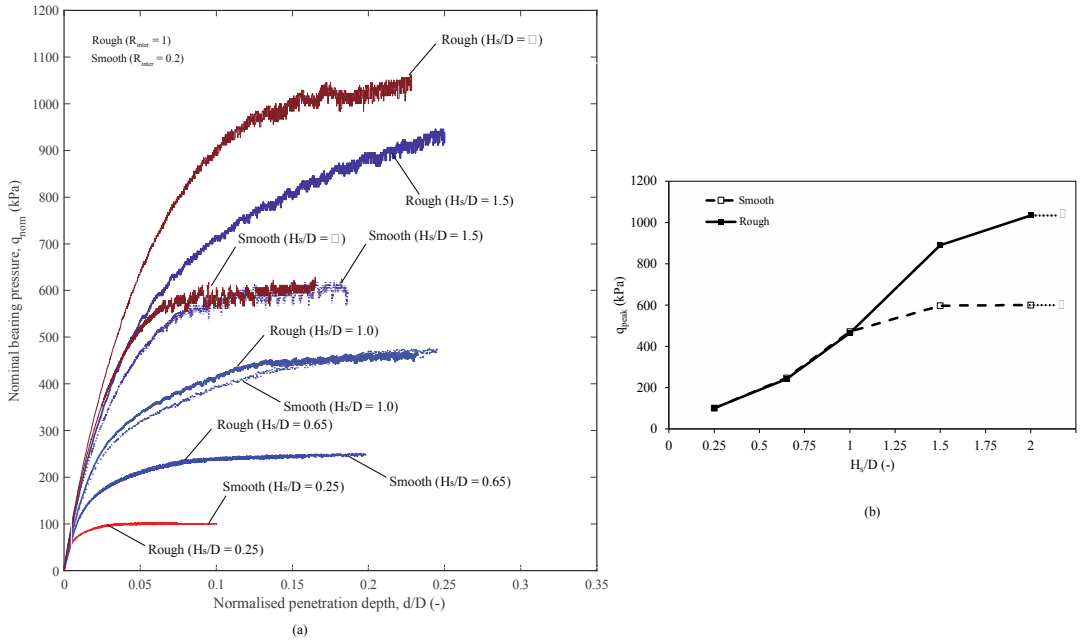

Figure 5 Effect of foundation roughness on the measured load-penetration response (H_s/D = 0.25-1.5, H_c/D = 0.5, D = 12 m, $\varphi' = \varphi'_b = 30^o$, $\psi = \psi_b = 2^o$, s_u = 10 kPa; tests G3 (T1-T4), G1 (T2, T6, T7), G4T2 of Table 3).

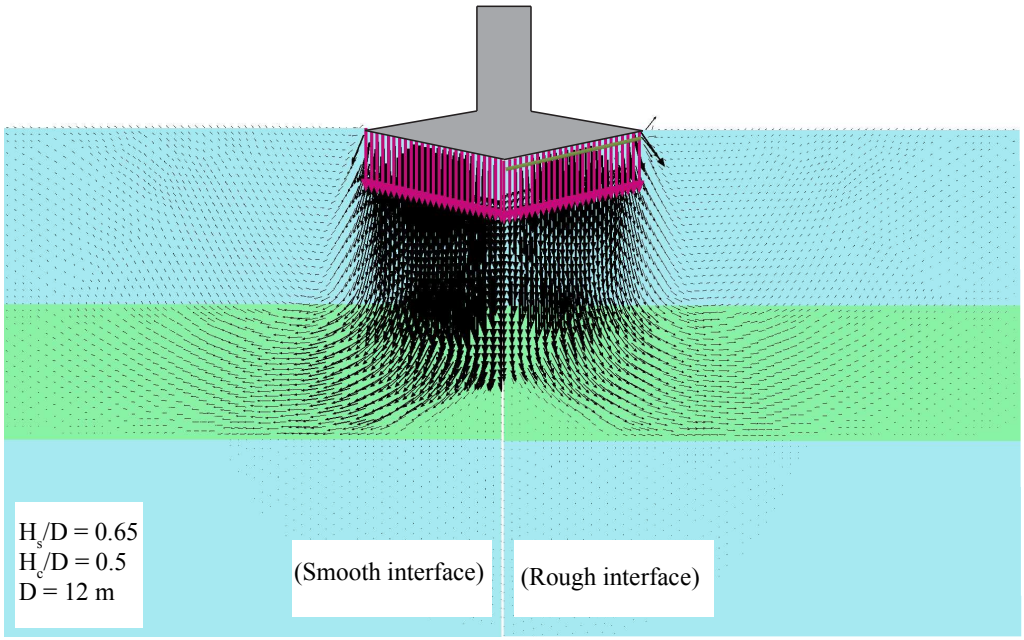

Figure 6a Effect of foundation roughness on the failure mechanism for relatively thin top sand (H_s/D = 0.65, H_c/D = 0.5, D = 12 m, $\varphi' = \varphi'_b = 30^o$, $\psi = \psi_b = 2^o$, s_u = 10 kPa; tests G1T2 (rough) and G3T2 (smooth) of Table 3).

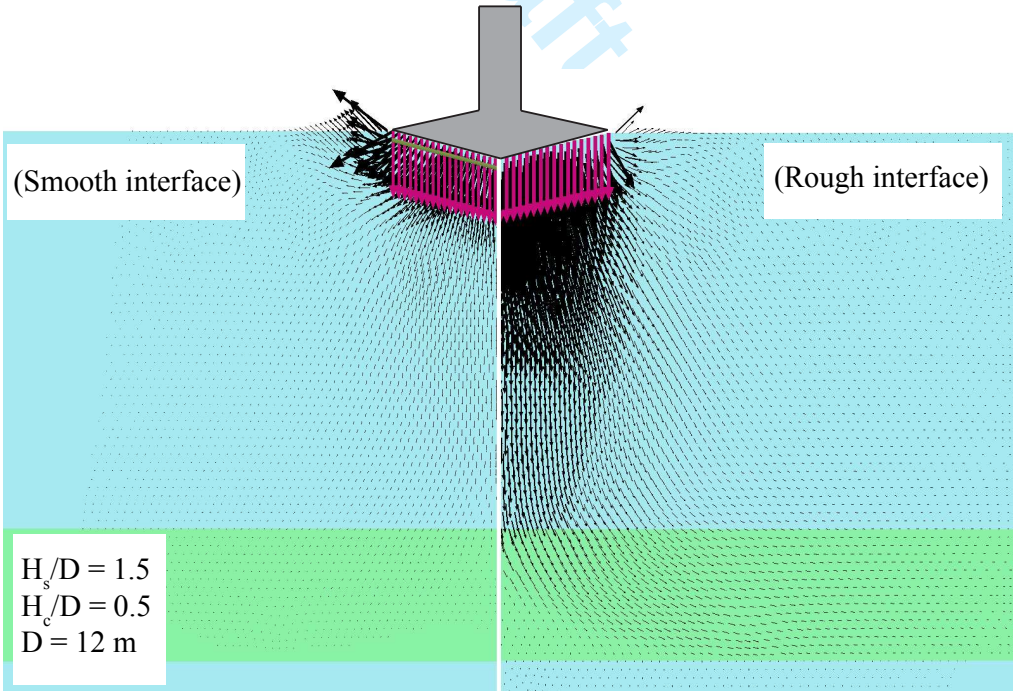

Figure 6b Effect of foundation roughness on the failure mechanism for relatively thicker top sand (H_s/D = 1.5, H_c/D = 0.5, D = 12 m, $\varphi' = \varphi'_b = 30^o$, $\psi = \psi_b = 2^o$, s_u = 10 kPa; tests G3T4 (smooth) and G4T7 (rough) of Table 3).

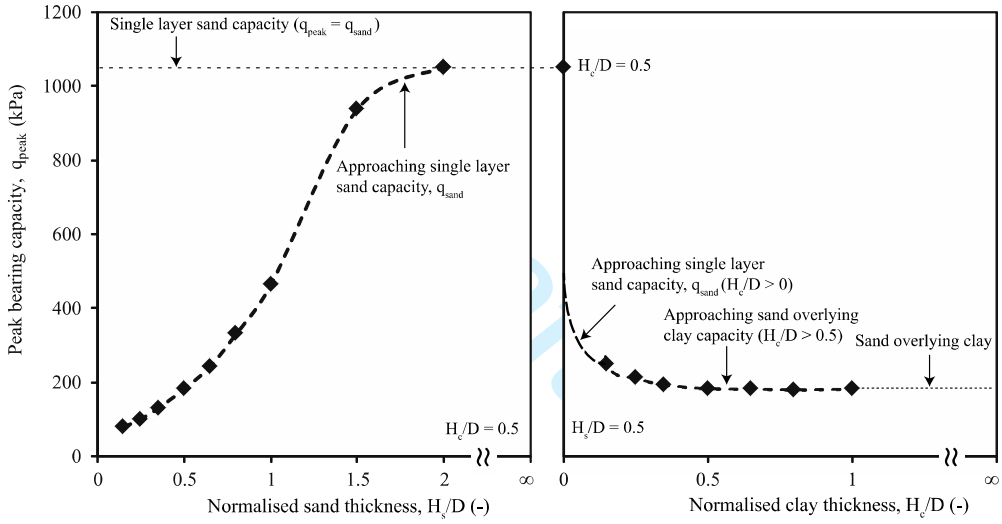

Figure 7 Effect of normalised geometries on the peak punch-through capacity a) effect of H_s/D (H_c/D = 0.5, D = 12 m, $\varphi' = \varphi'_b = 30^o$, $\psi = \psi_b = 2^o$, s_u = 10 kPa; tests G4 of Table 3) and b) effect of H_c/D (H_s/D = 0.5, $\varphi' = \varphi'_b = 30^o$, $\psi = \psi_b = 2^o$, s_u = 10 kPa; tests G5 of Table 3).

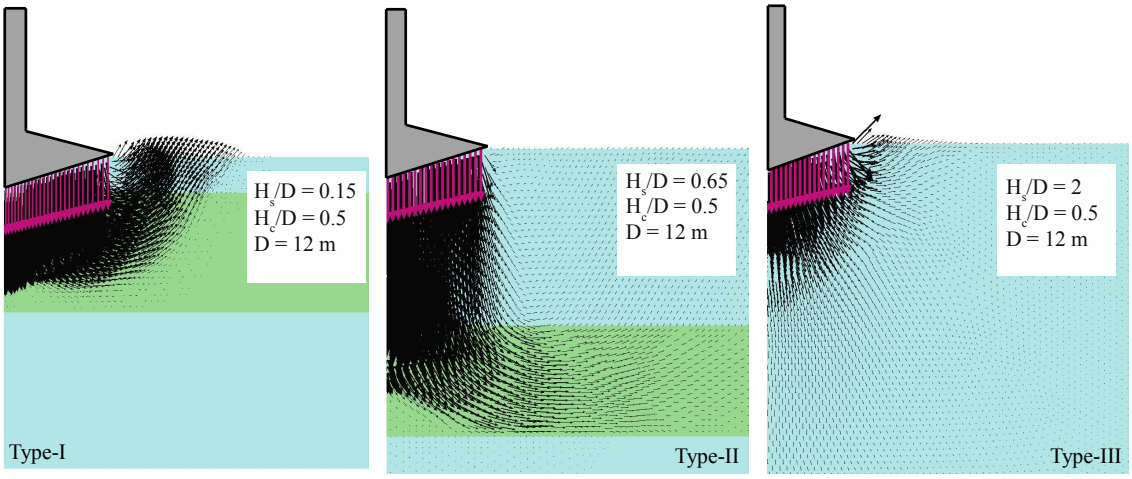

Figure 8 Effect of normalised top sand thickness (H_s/D) on the observed failure mechanism: a) small H_s/D (= 0.15) b) intermediate H_s/D (= 0.65) and c) large H_s/D (= 2) (in all cases, H_c/D = 0.5, D = 12 m, $\varphi' = \varphi'_b = 30^o$, $\psi = \psi_b = 2^o$, s_u = 10 kPa; tests G4T1, G1T2, G4T8 of Table 3).

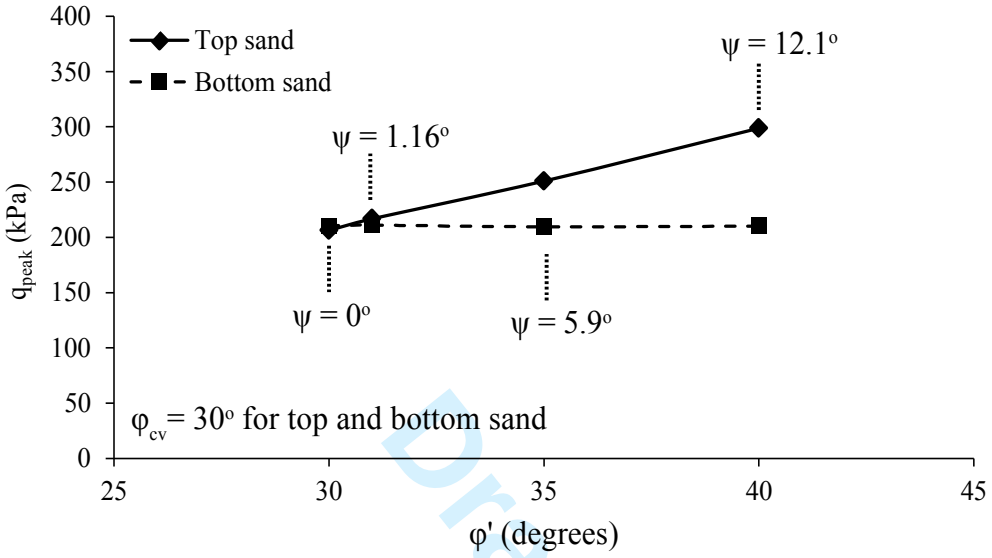

Figure 9 Effect of top and bottom sand operative friction and dilation angle on q_{peak} (H_s/D = 0.5, H_c/D = 0.25, φ_{cv} = 30°, s_u = 10 kPa; tests G6 and G9 of Table 3)

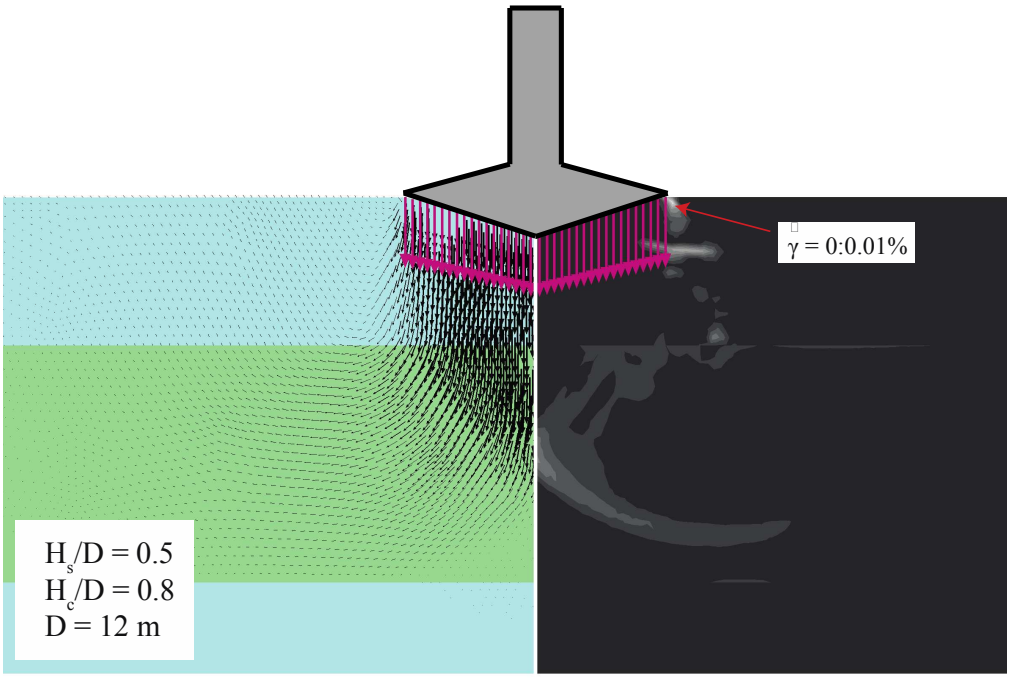

Figure 10a Effect of normalised clay thickness (H_c/D) on the failure mechanism: thick clay effect (H_s/D = 0.5, H_c/D = 0.8, D = 12 m, $\varphi' = \varphi'_b = 30^o$, $\psi = \psi_b = 2^o$, s_u = 10 kPa; test G5T6 of Table 3).

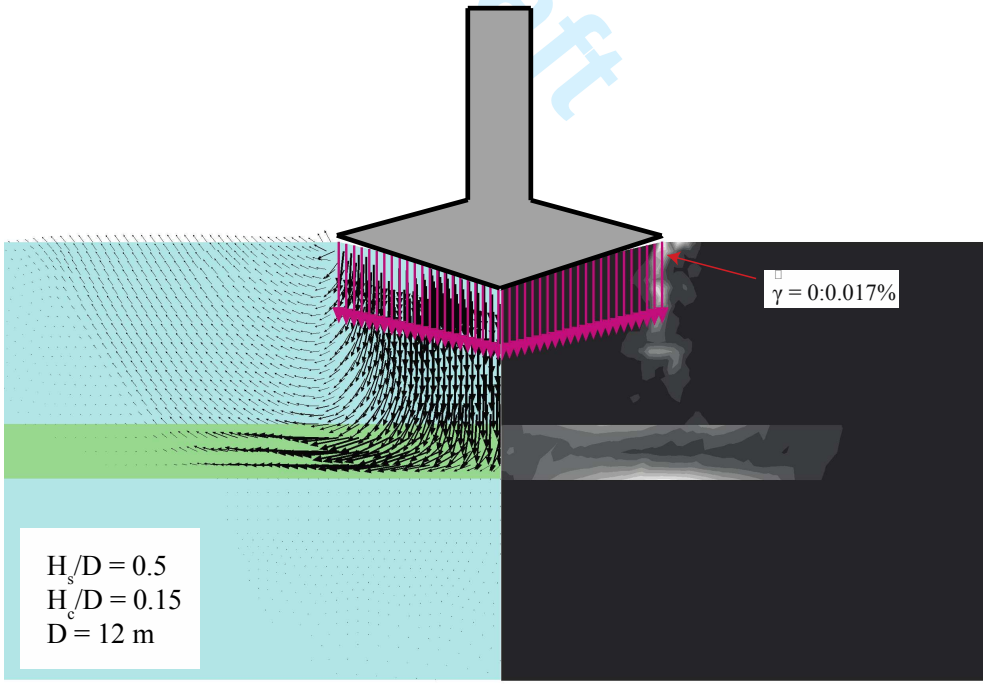

Figure 10b Effect of normalised clay thickness (H_c/D) on the failure mechanism: thin clay effect (H_s/D = 0.5, H_c/D = 0.15, D = 12 m, $\varphi' = \varphi'_b = 30^o$, $\psi = \psi_b = 2^o$, s_u = 10 kPa; test G5T1 of Table 3)

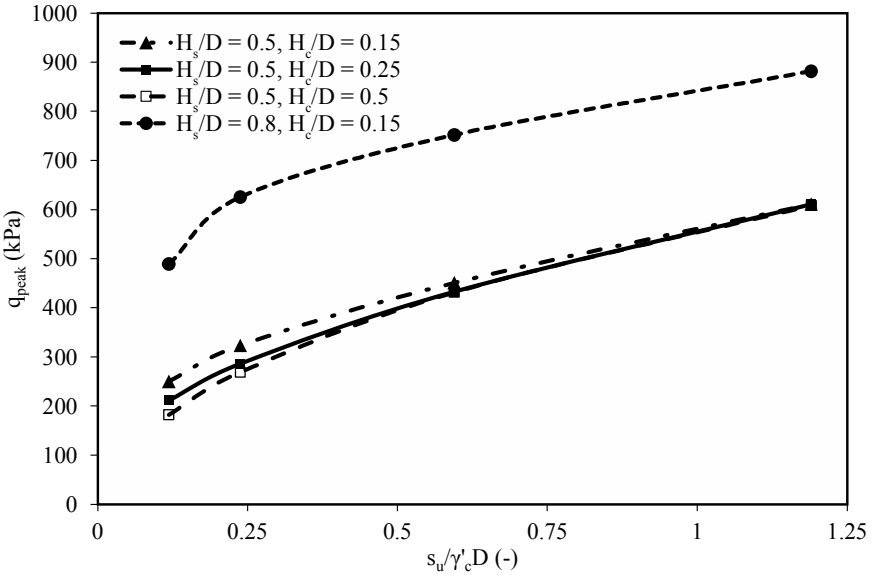

Figure 11 Effect of undrained clay strength s_u on q_{peak} (H_s/D = 0.5- 0.8, H_c/D = 0.15-0.25, D = 12 m, $\varphi' = \varphi'_b = 30^o$, $\psi = \psi_b = 2^o$, s_u = 10-100 kPa; tests G7 of Table 3).

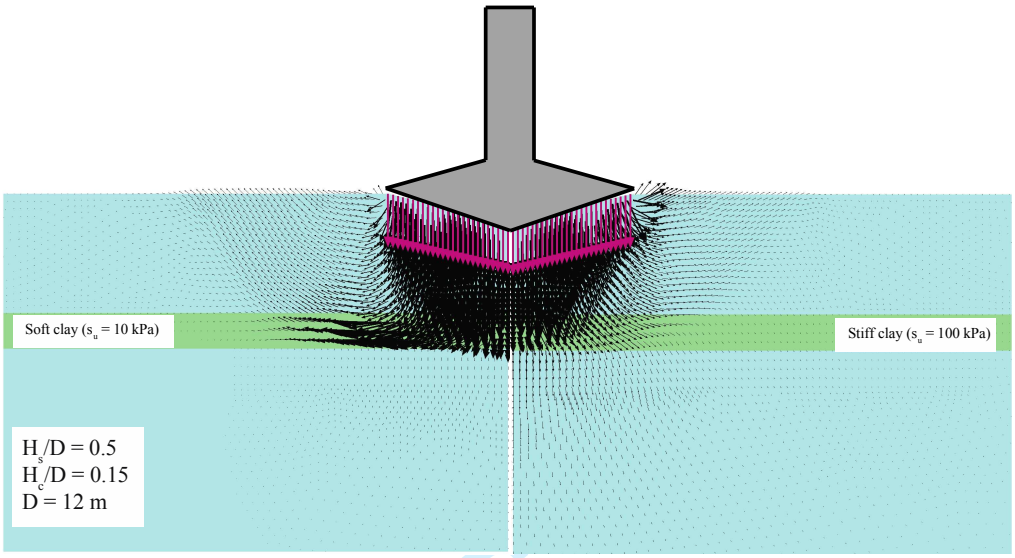

Figure 12 Soil flow mechanisms: effect of s_u (H_s/D = 0.5, H_c/D = 0.15, D = 12 m, $\varphi' = \varphi'_b = 30^o$, $\psi = \psi_b = 2^o$, s_u = 10kPa (left) and 100 kPa (right); tests G5T1 (left) and G7T9 (right) of Table 3).

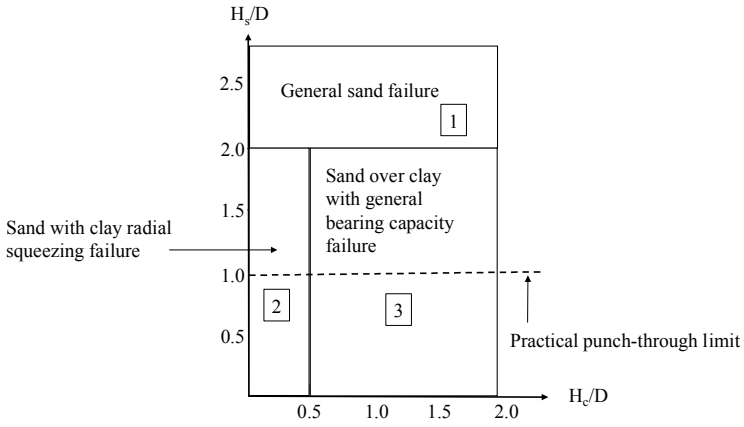

Figure 13 Possible failure zones in sand with interbedded clay

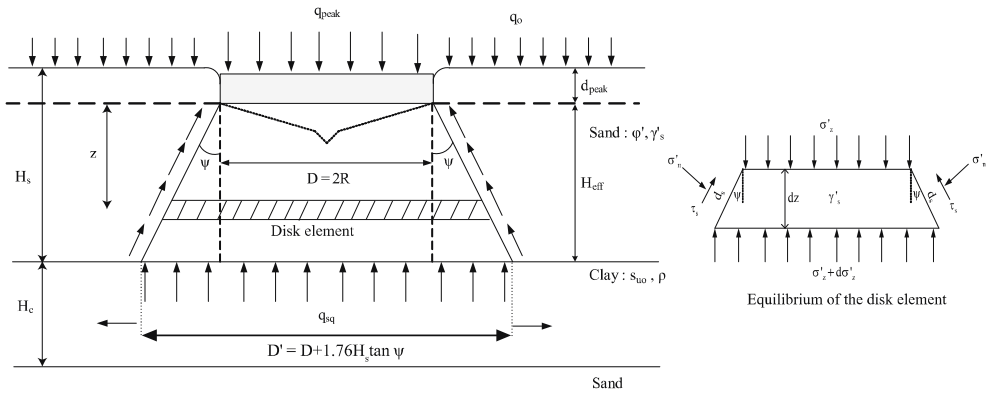

Figure 14 Analytical model of foundation bearing capacity in sand with a thin interbedded clay layer.

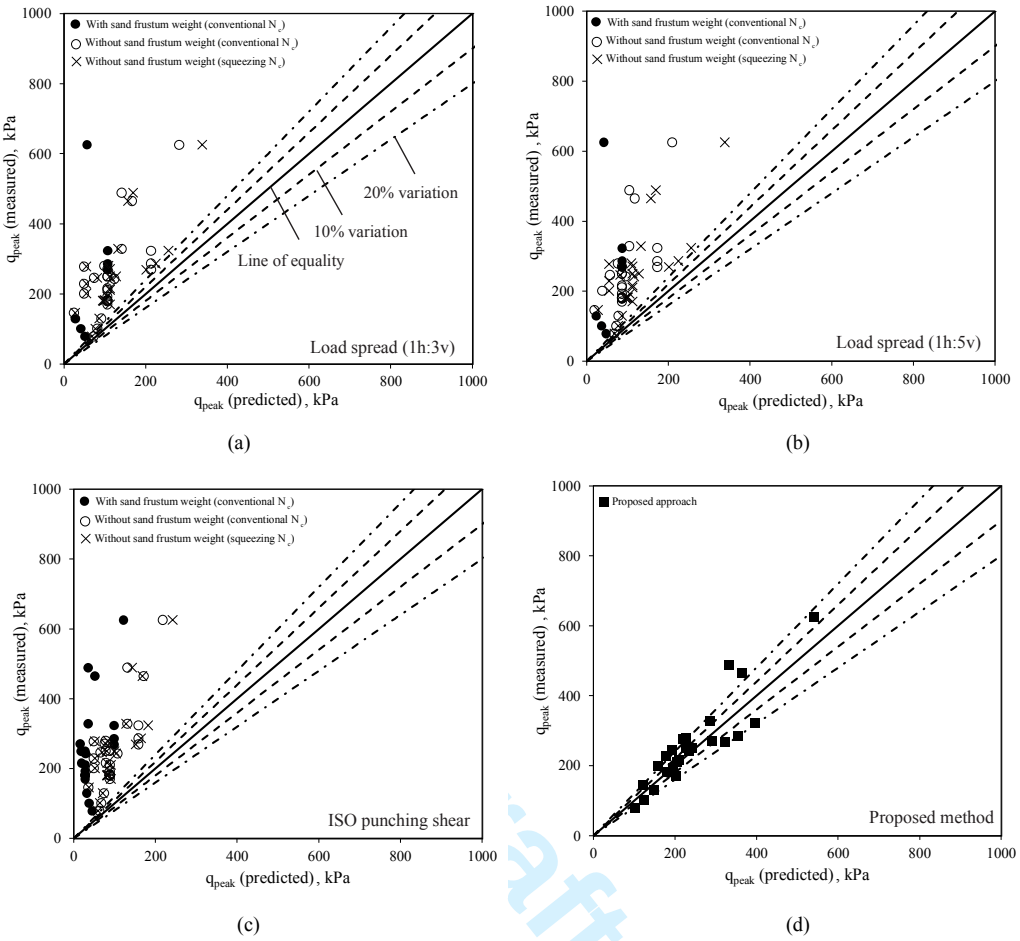

Figure 15 Performance of the developed model in comparison to ISO ($H_c/D \leq 0.5$): a) load spread approach (1h:3v), b) load spread approach (1h:5v), c) ISO punching shear approach, d) proposed method.

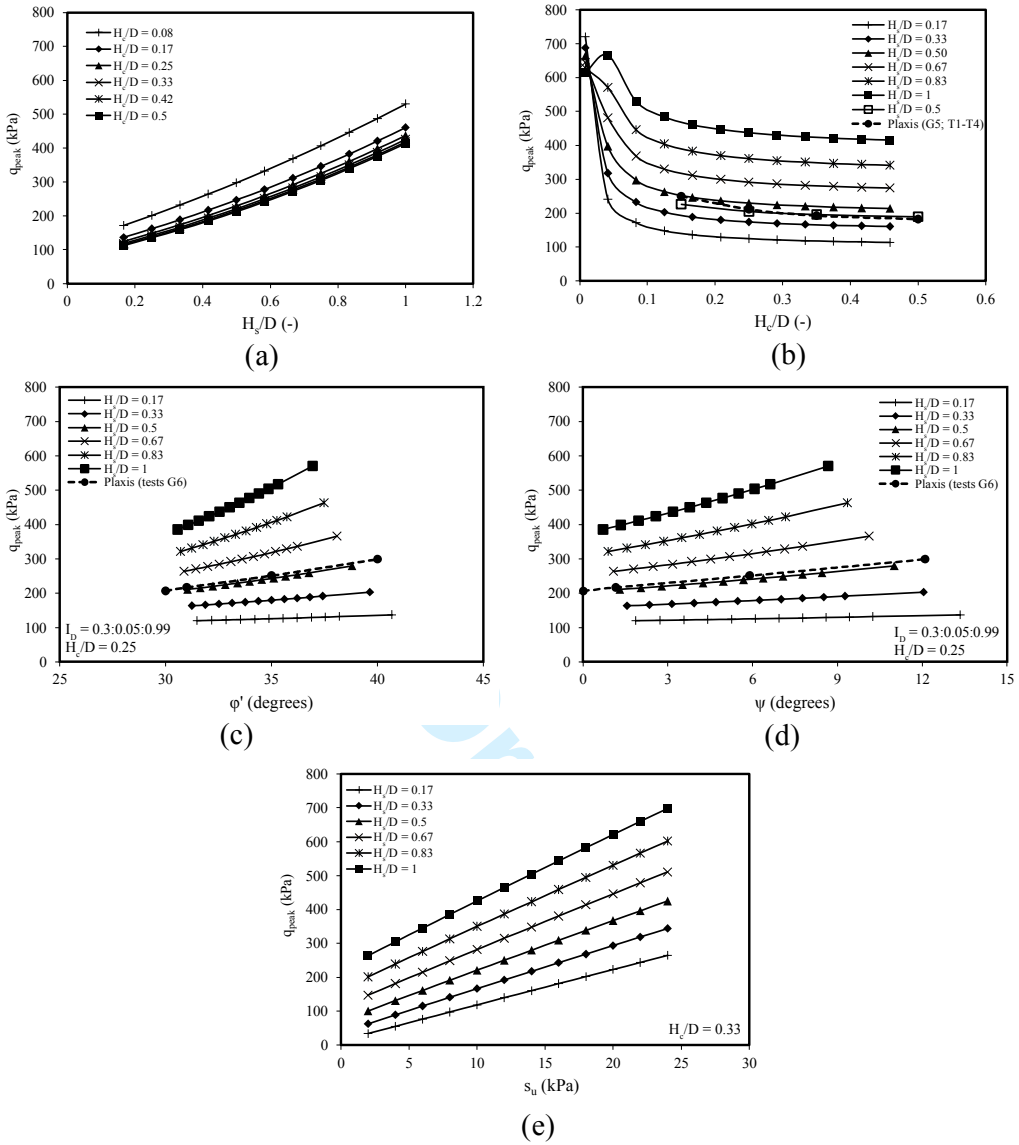

Figure 16 Effect of different parameters on q_{peak} in sand-clay-sand a) effect of H_s/D (D = 12 m, I_D = 50%, s_u = 10 kPa, φ_{cv} = 30°), b) effect from H_c/D (D = 12 m, I_D = 50%, s_u = 10 kPa, φ_{cv} = 30°), c) effect of top sand operative friction angle φ' (H_c/D = 0.25, D = 12 m, I_D = 0.3:0.05:0.99, s_u = 10 kPa, φ_{cv} = 30°), d) effect of top sand dilation angle ψ (H_c/D = 0.25, D = 12 m, I_D = 30% : 5% : 99%, s_u = 10 kPa, φ_{cv} = 30°) and e) effect of clay undrained shear strength s_u (H_c/D = 0.33, D = 12 m, I_D = 50%, φ_{cv} = 30°).

Table 1 Soil parameters used in the parametric study

Soil model	Parameter	Values
Sand (Hardening soil)	E_{50}^{ref} : MPa	24
	E_{oed}^{ref} : MPa	24
	E_{ur} : MPa	72
	e_o	0.5
	e_{min}	0.45
	e_{max}	0.74
	γ'_s :kN/m^3	10
	ν_s	0.2
	m	0.5
	p_{ref} : kPa	100
	R_{inter}	1
Clay (Tresca soil)	E/s_u	350 (after Das, 2010)
	γ'_c :kN/m^3	7
	ν_c	0.49

Note: ν_s= sand Poisson's ratio and ν_c= clay Poisson's ratio

γ'_s = effective unit weight of sand, γ'_c = effective unit weight of clay

Table 2 Centrifuge test details for FE model verification.

Test	Foundation	H_s (m)	H_c (m)	D (m)	H_s/D (-)	H_c/D (-)	φ' (^{o})	φ_{cv} (^{o})	ψ (^{o})	I_D (%)	s_{uo} (kPa)	ρ (kPa/m)	Comments
D1F30a	Flat footing	6.20	∞	6	1.03	∞	36.72	31	7.15	92	17.70	2.10	
D1F50a	Flat footing	6.20	∞	10	0.62	∞	37.86	31	8.57	92	17.70	2.10	Dense sand*
D1F70a	Flat footing	6.20	∞	14	0.44	∞	38.50	31	9.38	92	17.70	2.10	
L1SP4	Spudcan	6.00	∞	12	0.50	∞	33.27	31	2.84	43	12.96	1.54	
L3SP2	Spudcan	3.20	∞	8	0.40	∞	33.67	31	3.34	43	11.01	1.55	Loose sand*
L3SP3	Spudcan	3.20	∞	12	0.27	∞	33.80	31	3.50	43	11.01	1.55	

* Dense sand and loose sand data from Lee et al. (2013a) and Hu et al. (2014) respectively.

Table 3 Details of numerical simulation undertaken in this study**.

Test groups/tests		H_s (m)	H_c (m)	D (m)	H_s/D (-)	H_c/D (-)	φ' (°)	ψ (°)	φ'_b (°)	ψ_b (°)	s_u or s_{uo} (kPa)	ρ (kPa/m)	E_{50}^{ref} (MPa)	m (-)	R_{inter} (-)	Study focus
G1	T1, T2*, T3, T4	7.8	6	12	0.65	0.5	30	2	30	2	10	0	*10, 24, 30, 50*	0.5	1	Effect of sand stiffness.
G2	T1, T2, T3	7.8	6	12	0.65	0.5	30	2	30	2	10	0	30	*0, 0.75, 1*	1	Effect of stress dependency exponent m.
G3	T1, T2 T3, T4	*3, 7.8, 12, 18*	6	12	0.25, 0.65, 1, 1.5	0.5	30	2	30	2	10	0	24	0.5	0.2	Effect of foundation roughness.
G4	T1*, T2*, T3*, T4*, T5*, T6*, T7, T8, T9	*1.8, 3, 4.2, 6, 9. 6, 12, 18, 24,* ∞	6	12	0.15, 0.25, 0.35, 0.5, 0.8, 1, 1.5, 2, ∞	0.5, 0.5, 0.5, 0.5, 0.5, 0.5, 0.5, 0.5, 0	30	2	30	2	10	0	24	0.5	1	Effect of top sand thickness.
G5	T1*, T2*, T3*, T4*, T5*, T6*, T7*	6	*1.8, 3, 4.2, 6, 7.8, 9.6, 12*	12	0.5	0.15, 0.25, 0.35, 0.5, 0.65, 0.8, 1	30	2	30	2	10	0	24	0.5	1	Effect of clay thickness.
G6	T1*, T2*, T3*, T4*	6	3	12	0.5	0.25	*30, 31, 35, 40*	*0, 1.16, 5.9, 12.1*	30	2	10	0	24	0.5	1	Effect of top sand friction angle.
G7	T1*, T2, T3, T4*, T5, T6, T7*, T8, T9, T10*, T11*, T12, T13	6	6	12	0.5	0.5	30	5	30	2	*20, 50, 100 20, 50, 100 20, 50, 100 10, 20, 50, 100*	0	24	0.5	1	Effect of clay undrained shear strength.
G8	T1*, T2*	7.8	2.4	12	0.65	0.2	30	2	30	2	4	*1, 3*	24	0.5	1	Effect of clay strength non-homogeneity.
G9	T1, T2* T3, T4	7.8	2.4	12	0.65	0.2	30	2	*20, 30, 35, 40*	2	8	0	24	0.5	1	Effect of bottom sand friction angle.
G10	T1*, T2*, T3*	7.8	2.4	12	0.65	0.2	30	2	30	2	*2, 4, 6*	0	24	0.5	1	Additional analyses for model verification in soft clay.

**Note: Changing soil parameters within a group are in *Italic*. In all tests the normalised bottom clay thickness $H_b/D = 5$.

* Tests marked with an asterisk (29 in total) are included in the performance appraisal of the developed model.

Table 4 Comparison of q_{sand} among various methods for a rough foundation in sand with $\varphi' = 30^o$

φ' (^{o})	s_q (-)	s_γ (-)	d_q (-)	d_γ (-)	K_p* (-)	N_q (-)	N_γ (-)	d (m)	D (m)	d/D (-)	γ'_s (kN/m^3)	q_o (kPa)	q_{sand} (kPa)	q_{sand} (FE): rough (kPa)	q_{sand}** (FE): smooth (kPa)	β (^{o})	% discrepancy		Reference
																	rough	smooth	
30	1.3	1.3	1.03	1.03	3	18.40	15.67	2	12	0.2	10	24	1837	1034	516	180	78	-	Meyerhof (1963)
30	1.5	0.6	1.06	1.00	3	18.40	15.07	2	12	0.2	10	24	1243	1034	516	180	20	-	Hansen (1970)
30	1.5	0.6	1.06	1.00	3	18.40	22.40	2	12	0.2	10	24	1507	1034	516	180	46	-	Vesic (1975)
30	-	-	-	-	-	29.50	7.10	2	12	0.2	10	24	1134	1034	516	180	-	120	Bolton and Lau (1993) (smooth)
30	-	-	-	-	-	29.50	31.90	2	12	0.2	10	24	2622	1034	516	180	154	-	Bolton and Lau (1993) (rough)
30	1	1	1	1	3	18.40	21.35	2	12	0.2	10	24	1722	1034	516	180	67	-	Michalowski (1997) Upper bound (rough)
30	1	1	1	1	3	18.40	10.97	2	12	0.2	10	24	1100	1034	516	180	-	113	Michalowski (1997) Upper bound (smooth)
30	1	1	1	1	3	18.40	14.37	2	12	0.2	10	24	1304	1034	516	154	26	-	Cassidy and Houlsby (2002) (rough)
30	1	1	1	1	3	18.40	14.13	2	12	0.2	10	24	1289	1034	516	180	25		Cassidy and Houlsby (2002) (rough)
30	1	1	1	1	3	18.40	7.02	2	12	0.2	10	24	863	1034	516	154	-	67	Cassidy and Houlsby (2002) (smooth)
30	1	1	1	1	3	18.40	6.95	2	12	0.2	10	24	858	1034	516	180	-	66	Cassidy and Houlsby (2002) (smooth)
30	-	1.4	-	1.88	-	-	15.9	2	12	0.2	10	24	2511	1034	516	180	143		Lyamin et al. (2007) (upper bound)
30	-	1.4	-	1.88	-	-	14.57	2	12	0.2	10	24	2301	1034	516	180	123		Lyamin et al. (2007) (lower bound)

* K_p is the passive lateral earth pressure coefficient

** $R_{inter} = 0.1$

Table 5 Model performance indicators

Method name	$\frac{q_{peak}\ (measured)}{q_{peak}(predicted)}$ N_c (general) / N_c (squeezing)				
	Minimum	Maximum	Mean	SD	COV
ISO (2012): Projected area with spread ratio of 1h:3v	1.08/1.15	5.92/5.34	2.42/2.31	1.25/1.07	0.52/0.46
ISO (2012) Projected area with spread ratio of 1h:5v	1.16/1.24	7.66/6.91	3.08/2.93	1.68/1.45	0.54/0.49
ISO (2012): Punching shear	1.26/1.33	5.71/5.33	2.74/2.67	1.05/0.95	0.38/0.35
Proposed model	0.77	1.47	1.04	0.18	0.17

Note: h means horizontal and v stands for vertical. (29 tests in total).

For ISO methods only best estimates are included, neglecting the sand frustum weight.